

Nanoscale Horizons

Accepted Manuscript



This is an *Accepted Manuscript*, which has been through the Royal Society of Chemistry peer review process and has been accepted for publication.

Accepted Manuscripts are published online shortly after acceptance, before technical editing, formatting and proof reading. Using this free service, authors can make their results available to the community, in citable form, before we publish the edited article. We will replace this *Accepted Manuscript* with the edited and formatted *Advance Article* as soon as it is available.

You can find more information about *Accepted Manuscripts* in the [Information for Authors](#).

Please note that technical editing may introduce minor changes to the text and/or graphics, which may alter content. The journal's standard [Terms & Conditions](#) and the [Ethical guidelines](#) still apply. In no event shall the Royal Society of Chemistry be held responsible for any errors or omissions in this *Accepted Manuscript* or any consequences arising from the use of any information it contains.

Photocatalytic conversion of CO₂ over graphene-based composites: current status and future perspective

 Min-Quan Yang,^{a,b} and Yi-Jun Xu*^{a,b}

 Received 00th January 20xx,
Accepted 00th January 20xx

DOI: 10.1039/x0xx00000x

www.rsc.org/

The continuous rise in atmospheric CO₂ level and ever-increasing demand of energy have raised serious concerns about the ensuing effects on the global climate change and future energy supply. Photocatalytic conversion of CO₂, which uses solar light energy to recycle CO₂ into fuels and chemicals, provides a promising and straightforward strategy to simultaneously reduce the atmospheric CO₂ level and fulfil the future energy demand. However, the lack of substantial development of state-of-the-art materials remains a major bottleneck of this technology. In recent years, graphene-based composite photocatalysts have gained increasing interests in CO₂ conversion due to the introduction of graphene with a series of unique physicochemical properties, which has shown significant role for promoting the photocatalytic solar energy conversion efficiency. In this review, we comprehensively summarize the typical literature reports of graphene-based composites for photocatalytic conversion of CO₂ to produce solar fuels and chemicals. The main types of the reported graphene-based composites and the effect of graphene in the composites for improving the photocatalytic performance have been elaborated. In particular, we have highlighted the possible role of graphene in tuning the product selectivity of photocatalytic reduction of CO₂. Finally, perspectives on the existing problems and future research of graphene-based composites toward photocatalytic conversion of CO₂ are critically discussed.

1. Introduction

The rapid development of human society since the Industrial Revolution has resulted in a dramatically raise of global demand for energy, which has increased from the average energy consumption rate of 2.8 terawatt (TW) in 1950 to 15 TW in 2010, and is projected to increase to 25–27 TW by 2050.^{1–3} Fossil fuels, as the most important global energy source with the advantages such as being freely provided by nature, high energy content, and ease of transportation and storage, have accounted for the largest proportion, more than 80 percent, of the energy supply of current world.^{1–3} The heavy reliance on fossil fuels for the production of energy leads to an explosive growth of CO₂ emission into the atmosphere, which has disturbed the balance of natural cycle of CO₂ emission and uptake (fixation by terrestrial plants and microorganisms, plus underground inorganication),¹ and caused a severe global climate change,^{1,4} resulting in a devastating impact on the living environment of humans. Additionally, the fast increase in combustion of fossil fuels also leads to an excessive exploitation and sharp depletion of the finite global fossil fuel reserves, causing serious energy shortage crisis throughout the world since the late 1970s.⁵ The ever-increasing environmental issue and lack of natural energy

resources have raised serious concerns about the ensuing effects on the global energy security, environmental security, and economic security *etc.*⁶ Alleviating the environmental burden and seeking alternative sustainable energy supply have become the most urgent tasks of human society.

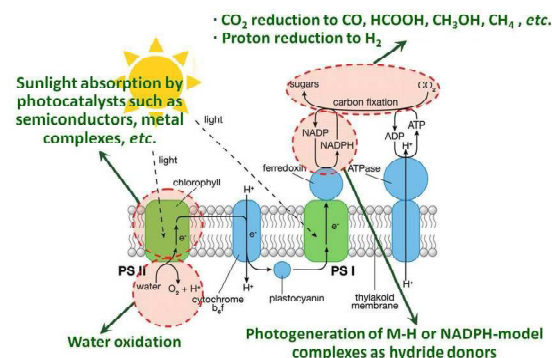


Fig. 1 Schematic diagram of a natural photosynthetic system, with four areas of artificial photocatalysis research highlighted in red and described in green text. The artificial photocatalytic systems are designed to perform similar functions to the different components of natural photosystems, which typically focuses on one or two of these topics at a time to reduce complexity. The goal of photocatalytic reduction of CO₂ is to mimic the natural photosynthetic system for generation of renewable fuels and chemicals such as CO, formic acid, methanol and methane from CO₂, H₂O, and sunlight. Reprinted with permission from ref 4. Copyright 2010 American Chemical Society.⁴

In this context, semiconductor photocatalysis, a well-orchestrated mimic of natural photosynthesis (**Fig. 1**) reported from 1960s⁷ for direct converting solar energy to

^a State Key Laboratory of Photocatalysis on Energy and Environment, College of Chemistry, Fuzhou University, Fuzhou, 350002, P. R. China.

^b College of Chemistry, New Campus, Fuzhou University, Fuzhou, 350108, P. R. China; E-mail: yixu@fzu.edu.cn

chemical energy, is likely to kill these two birds with one stone. In particular, in 1979, Inoue *et al.* for the first time observed the photocatalytic reduction of CO₂ in aqueous suspensions of semiconductor photocatalysts such as TiO₂, ZnO, CdS, GaP and SiC for generation of methane, methanol, formaldehyde and formic acid,⁸ which are high energy density fuels (*e.g.*, methane, methanol)^{2, 6} compatible with current energy infrastructure and carbon feedstocks (*e.g.*, formaldehyde and formic acid)^{1, 6} available for chemical synthesis. The photocatalytic technique shows a fascinating potential of recycling CO₂ from a climate altering waste product into value-added chemicals, which has been regarded as a promising way to simultaneously address the global energy and environment issues.

Over the past decades, continuous efforts have been devoted to the photocatalysis research. A large number of new photocatalyst materials have been developed and studied for diverse photocatalytic processes,^{1, 9-17} including the photocatalytic reduction of CO₂ to produce solar fuels and chemicals.^{1, 4, 6, 15-20} However, despite the significant progresses made in this area, the state-of-the-art development of photocatalysis still suffers from some severe limitations such as inferior utilization of solar light, low quantum efficiency, instability of some photocatalysts (*e.g.*, metal sulfides) and hard control of the product selectivity of some reactions (*e.g.*, photocatalytic reduction of CO₂). To overcome these challenges, different strategies including metal loading, ion doping, crystal structure, particle size and morphology controlling, and carbonaceous nanomaterials modification, *etc.* have been explored.²¹⁻²⁷

In recent years, graphene, a two-dimensional (2D) single layer of graphite with exceptional electrical, thermal, optical, and mechanical properties,²⁸⁻³⁵ has triggered a surge of research interest in both scientific and technological communities. The fabrication of graphene-based composite materials has evolved into myriad fields, including nanoelectronics, bio-sensors, energy storage and conversion, optoelectronics and supercapacitors, *etc.*³⁶⁻³⁸ In particular, the past several years have witnessed the cornucopia of the fabrication of graphene-based composite photocatalysts for improving the solar energy conversion efficiency.³⁹⁻⁵⁸ The large specific surface area, good optical transmittance, high work function and excellent electronic conductivity of graphene make it to be a high performance candidate for catalyst support and electron acceptor/trapper.^{29, 59, 60} Up to date, more than 200 different kinds and over 2000 publications of graphene-based composite photocatalysts have been reported. In these literature reports, it is notable that the integration of appropriate amount of graphene with the photoactive components obviously improves the efficiency of graphene-based composite photocatalysts toward the solar energy conversion, although the real state of graphene in the composite photocatalysts is different from that of the original defined single-layer and defect-free graphene due to the presence of defect, oxygenated functional groups and aggregation of the graphene sheets,^{29, 60} which makes it

hard to take full advantages of the excellent electronic, optical and physicochemical properties of graphene. Such situation strongly suggests that (i) the integration of graphene with photoactive ingredient (*e.g.*, semiconductor) to form new multicomponent composite materials provides a promising way for constructing the next-generation artificial photosynthetic systems; (ii) there is still a large room to improve the performance of graphene-based composite photocatalysts by optimizing the physicochemical properties of the prepared graphene in the composites.

During the past years, some reviews have been published in literature pertaining to the preparation and/or application of graphene-based composites.⁶¹⁻⁶⁶ However, most of them give little attention or even neglect to cover the reaction type of photocatalytic reduction of CO₂. Very recently, Low *et al.*, have discussed the important advantages of coupling graphene with a photocatalyst for promoting the catalytic reduction of CO₂ with some selected reports,⁶⁷ but the comprehensive summary of the literature results of graphene-based composites for photocatalytic conversion of CO₂ to produce solar fuels and chemicals is still unavailable in the literature. In particular, none of the previous reviews have highlighted the role of graphene in tuning the product selectivity for photocatalytic CO₂ conversion, which is of great significance for promoting the development of photocatalytic solar fuel production. Therefore, facing the increasing research interest of this field in recent years, it is desirable and necessary to present an up-to-date insightful review of photocatalytic reduction of CO₂ to produce solar fuels and chemicals over graphene-based photocatalysts, with the purpose of describing the current state and promoting further development in this area.

As such, in this critical review, we comprehensively summarize the results of graphene-based composites for photocatalytic conversion of CO₂ from the following aspects. Firstly, we briefly illustrate the fundamentals of photoactivity enhancement of graphene-based composites for catalytic conversion of CO₂ to solar fuels and chemicals. Secondly, after the collection of the literature reports of graphene-based composites for photocatalytic reduction of CO₂, the main types of these developed graphene-based composites and the effect of graphene in these composites for improving the photocatalytic performance are elaborated with selected typical examples. Thirdly, the significant effect of graphene in tuning product selectivity for photocatalytic reduction of CO₂ is discussed. Finally, the challenges and issues confronted by graphene-based photocatalysts for reduction of CO₂ and perspectives on future research have been presented.

2. Fundamentals of photoactivity enhancement of CO₂ reduction over graphene-based composites

As CO_2 is a thermodynamically stable and chemically inert molecule with σ - and π -bond characteristics and linear molecular structure of $\text{O}=\text{C}=\text{O}$, the reduction of CO_2 is energetically uphill and highly endothermic. As schematically illustrated in Fig. 2, the standard Gibbs free energies (ΔG^0) for the reduction of CO_2 with water to carbon monoxide, methanol, methane, formaldehyde and formic acid are all highly positive,⁶⁸ indicating that in order to convert CO_2 into value-added chemicals and fuels, large amount of external energy input is required, which is indispensable for overcoming the reaction barriers to break the $\text{C}=\text{O}$ bond and promote the formation of C-H/C-C bond and then the final chemical products.

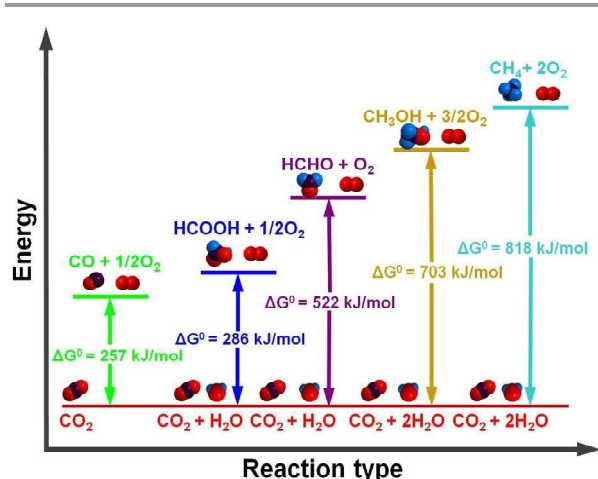


Fig. 2 Energy diagram for conversion of CO_2 into chemical products.

In photocatalytic reduction of CO_2 , solar light is adopted as the input energy source to trigger the CO_2 reduction with H_2O through the employment of appropriate robust and efficient photocatalysts. The primary processes of catalytic reduction of CO_2 over traditional photocatalysts have been shown in Fig. 3. Typically, under the light irradiation, the photoactive material (taking the most widely reported semiconductor as example) is excited to generate charge carriers (*i.e.* electron-hole pairs) upon the absorption of photons with energy equal to or higher than its band gap energy (E_g).^{1, 69, 70} Then, the spatially separated photogenerated electrons and holes would migrate to the catalytically active sites at the semiconductor surface (**Pathway 1 and 2**) and subsequently transfer to the adsorbed molecules (CO_2 and H_2O). The hole oxidizes the H_2O to O_2 and release H^+ , and the electrons reduce CO_2 by a sequence of reactions to produce chemicals and fuels such as CO , CH_3OH and CH_4 with the assistance of H^+ .²⁰ However, it is notable that the photogenerated carriers would also recombine in the bulk of the semiconductor (**Pathway 3**, volume recombination) or on the semiconductor surface with their trapped counterparts of opposite charge (**Pathway 4**, surface recombination),^{69, 70} which release the

light energy in the form of heat or photon. Both of these recombination processes are detrimental to the efficiency of photocatalysis.^{1, 70} They strongly compete with the processes of separation and transfer of photogenerated charge carriers, resulting in the low photocatalytic CO_2 reduction efficiency. Therefore, promoting the separation and transfer of photogenerated charge carriers and inhibiting their recombination are essential for improving the efficiency of photocatalytic solar fuels and chemicals production.

In the case of graphene-based composite photocatalysts, the integration of graphene with the photoactive ingredient (*e.g.*, semiconductor, organics) has widely proven to be effective for enhancing the separation and inhibiting the recombination of charge carriers.^{29, 59, 60} Graphene with high work function is able to act as an electron acceptor/trapper to induce electrons transfer from the photoactive ingredient to it,⁷¹⁻⁷³ leading to the formation of an additional non-radiative delay channel for the separation and migration of photogenerated charge carriers (**Pathway 5**), as depicted in the right of Fig. 3. Then, the good conductivity and high electron mobility of graphene promotes the transferred electrons to diffuse fast along its unique large 2D π -conjugated structure, which efficiently improves the probability and rate of the charge carriers (*i.e.* electron-hole pairs) transfer in the photocatalyst.

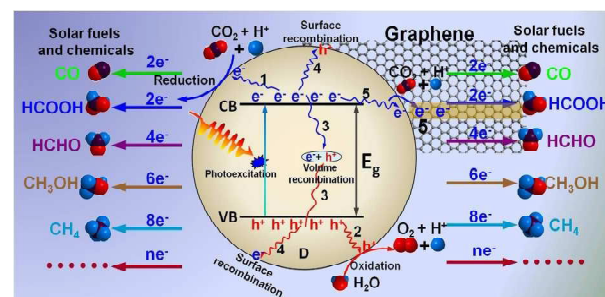


Fig. 3 Schematic illustration of photocatalytic reduction of CO_2 to solar fuels and chemicals in the presence of water over graphene-based composites (taking the most widely studied graphene-semiconductor photocatalysts as example). Note: VB refers to valance band, CB refers to conduction band, E_g refers to band-gap energy.

In addition, the graphene with large π -conjugated structure would enhance the adsorption of CO_2 due to that the CO_2 molecules also contain delocalized π -conjugation binding π_3^* ,^{74, 75} which can form strong π - π conjugation with graphene and thus increase the local concentration of CO_2 on the surface of the photocatalyst. Especially, the strong π - π conjugation between CO_2 and graphene can result in the destabilization and activation of CO_2 molecules.^{74, 75} Therefore, the integration of graphene with photoactive ingredient is not only able to enhance the separation and transfer of photogenerated charge carriers in the composite photocatalysts, but also can promote the photocatalytic reduction of CO_2 to be performed on the

graphene surface with low external energy, thereby significantly increasing the reaction sites and likelihood of photogenerated electrons to interact with the adsorbed CO₂ reactants. As a result, high photocatalytic activity of the graphene-based composite photocatalysts can be expected.

Moreover, the 2D structured graphene with high surface area is excellent catalyst supports. When it is utilized to integrate with the photoactive material, it is possible to promote the dispersion and inhibit the aggregation of the nanostructured photoactive component. This would result in the short diffusion length of photogenerated charge carriers and large reactive surface for interaction with adsorbed CO₂ molecules, and consequently, improved efficiency of photocatalytic solar fuels and chemicals production. Finally, in some cases, the integration of graphene with photoactive ingredient, such as typical TiO₂ semiconductor, could extend the light absorption range of the graphene-based composite photocatalysts. The broad light absorption is also beneficial for enhancing the utilization of solar energy and improving the efficiency of photocatalytic CO₂ conversion. Therefore, the integration of graphene with photoactive material is believed to provide a wide range of opportunities to prepare diverse new graphene-based composite materials with extraordinary properties for promoting the photocatalytic conversion of CO₂.

3. Summary and Category of Graphene-Based Composite Photocatalysts

Table 1 has summarized the typical reports in literature of photocatalytic reduction of CO₂ over graphene-based composite photocatalysts. An overview of the summary results shows that the graphene-based composites developed for photocatalytic reduction of CO₂ are mainly consisted of graphene-semiconductor photocatalysts, for which the semiconductor acts as light harvesters and graphene as co-catalyst. In addition, the combination of graphene-organics composites with enzyme for photocatalytic conversion of CO₂ to fuels and chemicals has also been reported, which forms the second type of graphene-organics/biomolecule photocatalysts. Moreover, some reports have shown that the graphene derivatives such as graphene oxide (GO) and nitrogen doped graphene are able to perform as semiconductors, which have proven to exhibit obvious photoactivity in reduction of CO₂. Therefore, they can be regarded as another new type of graphene derivatives-based photocatalysts.

Consequently, in terms of different photoactive components, the as-reported graphene-based composites in literature for photocatalytic reduction of CO₂ have been classified into three main groups: graphene-semiconductor photocatalysts, graphene-organics/biomolecule photocatalysts and graphene derivatives-based photocatalysts. In the following section, the typical examples of these different types of graphene-based composite photocatalysts and the effect of graphene in these composites for improving the photocatalytic performance have been discussed separately.

Table 1. Summary of photocatalytic conversion of CO₂ into solar fuels and chemicals over typical graphene-based composite photocatalysts.

Composite photocatalyst	Light source	Reaction medium	Main products	Photocatalytic performance	Ref. (Year)
¹ RGO-P25; ² SEG-P25	UV light, 100 W mercury vapor lamp; Visible light, 60 W daylight bulb	CO ₂ and H ₂ O vapor	CH ₄	UV light: 1.9 μmol m ⁻² h ⁻¹ , the photoactivity is close to that of TiO ₂ ; ² 8.5 μmol m ⁻² h ⁻¹ , 4.5-fold of TiO ₂ Visible light: 1.3 μmol m ⁻² h ⁻¹ , 2.3-fold of TiO ₂ ; ² 4.0 μmol m ⁻² h ⁻¹ , 7.2-fold of TiO ₂	76 (2011)
SEG-TiO ₂	UV light, 100 W mercury vapor lamp; Visible light, 60 W daylight bulb	CO ₂ and H ₂ O vapor	CH ₄	UV light: 9.3 μmol m ⁻² h ⁻¹ , 3.5-fold of TiO ₂ ; Visible light: 1.5 μmol m ⁻² h ⁻¹ , 3.7-fold of TiO ₂	77 (2012)
G-TiO ₂	—, 300 W xenon lamp	CO ₂ and H ₂ O vapor	CH ₄ , C ₂ H ₆	CH ₄ , 8 μmol h ⁻¹ g ⁻¹ ; C ₂ H ₆ , 16.8 μmol h ⁻¹ g ⁻¹ ; the total solar fuel production rate is 1.7-fold of TiO ₂	78 (2013)
G-Ti _{0.91} O ₂	—, 300 W xenon lamp	CO ₂ and H ₂ O vapor	CO, CH ₄	CO, 8.9 μmol h ⁻¹ g ⁻¹ ; CH ₄ , 1.1 μmol h ⁻¹ g ⁻¹ , the total solar fuel production rate is 7.1-fold of TiO ₂	79 (2012)
RGO-(g-C ₃ N ₄)	Visible light, 15 W daylight bulb	CO ₂ and H ₂ O vapor	CH ₄	0.59 μmol h ⁻¹ g ⁻¹ ; 2.3-fold of g-C ₃ N ₄	74 (2015)
RGO-CdS	Visible light, 300 W xenon lamp	CO ₂ and H ₂ O vapor	CH ₄	2.5 μmol h ⁻¹ g ⁻¹ ; 12-fold of CdS	75 (2014)
RGO-Cu ₂ O	Visible light, 150 W xenon lamp	CO ₂ saturated Na ₂ S solution	CO	50 ppm h ⁻¹ g ⁻¹ , 2-fold of Cu ₂ O	80 (2014)
RGO-WO ₃	Simulated solar light, 500 W xenon lamp	CO ₂ saturated NaOH solution	CH ₃ OH	4.2 μmol h ⁻¹ g ⁻¹ , 1.5-fold of Cu ₂ O	81 (2014)
	Visible light, 300 W	CO ₂ and H ₂ O vapor	CH ₄	0.11 μmol h ⁻¹ , the photoactivity of WO ₃	82

	xenon lamp			is negligible	(2013)
RGO-ZnO	Simulated solar light, 500 W xenon lamp	CO ₂ saturated NaHCO ₃ solution	CH ₃ OH	4.6 μmol h ⁻¹ g ⁻¹ ; 1.7-fold of ZnO	83
G-TiO ₂ -M, M = ¹ Au, ² Ag, ³ Pd, ⁴ Pt	Visible light, 15 W daylight bulb	CO ₂ and H ₂ O vapor	CH ₄	¹ 0.13, ² 0.17, ³ 0.2, ⁴ 0.28 μmol h ⁻¹ g ⁻¹ ; ¹ 6, ² 7.9, ³ 9.5, ⁴ 13.5-fold of TiO ₂	84
RGO-Ag-CdS	Visible light, 300 W xenon lamp	CO ₂ and H ₂ O vapor	CO, CH ₄	CO, 3.6 μmol h ⁻¹ g ⁻¹ ; CH ₄ , 1.2 μmol h ⁻¹ g ⁻¹ ; the total solar fuel production rate is 1.4-fold of RGO-CdS	85
RGO-Fe ₂ V ₄ O ₁₃ -CdS	Visible light, 300 W xenon lamp	CO ₂ and H ₂ O vapor	CH ₄	CH ₄ , 2.3 μmol h ⁻¹ g ⁻¹ ; 1.5-fold of Fe ₂ V ₄ O ₁₃ -CdS	86
RGO-Cu ₂ O-Au/Cu	Visible light, 300 W xenon lamp	CO ₂ saturated H ₂ O	CH ₃ OH	20.0 ppm cm ⁻² h ⁻¹ ; 7.8-fold of Cu ₂ O	87
RGO-NiO _x -Ta ₂ O ₅	UV-vis light irradiation, 400W metal halide lamp	CO ₂ and H ₂ O vapor	CH ₃ OH	0.46 μmol h ⁻¹ , 3.4-fold of NiO _x -Ta ₂ O ₅	88
G-MAQSP ^a	Visible light, 450 W xenon lamp	CO ₂ bubbled Na ₃ PO ₄ buffer with TEOA ^b	HCOOH	55.3 μmol h ⁻¹ , 2.4-fold of MAQSP	89
G-IP ^c	Visible light, 450 W xenon lamp	CO ₂ bubbled Na ₃ PO ₄ buffer with TEOA	CH ₃ OH	11.21 μmol h ⁻¹ , the photoactivity of IP is negligible	90
RGO-BODIPY ^d	Visible light, 450 W xenon lamp	CO ₂ bubbled Na ₃ PO ₄ buffer with TEOA	HCOOH	72.1 μmol h ⁻¹ , 11.4-fold of BODIPY	91
(B doped RGO)-P25	Simulated solar light, 300 W xenon lamp	CO ₂ saturated Na ₂ SO ₃ solution	CH ₄	1.3 μmol h ⁻¹ g ⁻¹ , 5.2-fold of P25	92
G-(N doped TiO ₂)	Visible light, 15 W daylight lamp	CO ₂ and H ₂ O vapor	CH ₄	0.37 μmol h ⁻¹ g ⁻¹ , 10.9-fold of N-TiO ₂	93
¹ G-THPP ^e ² G-CoTHPP ^f	Visible light, xenon lamp 100mW cm ⁻²	CO ₂ and H ₂ O vapor	CH ₄ , C ₂ H ₂	¹ CH ₄ , 57 μmol h ⁻¹ m ⁻² , C ₂ H ₂ , 113 μmol h ⁻¹ m ⁻² ; the total solar fuel production rate is 530-fold of THPP; ² CH ₄ , 38 μmol h ⁻¹ m ⁻² , C ₂ H ₂ , 42 μmol h ⁻¹ m ⁻² ; the total solar fuel production rate is 407-fold of CoTHPP	94
GO	Simulated solar light, 300 W halogen lamp	CO ₂ and H ₂ O vapor	CH ₃ OH	0.17 μmol h ⁻¹ g ⁻¹ , 5.7-fold of P25	95
GO-Cu	Visible light, 300 W halogen lamp	CO ₂ and H ₂ O vapor	CH ₃ OH, CH ₃ CHO	CH ₃ OH, 2.9 μmol h ⁻¹ , g ⁻¹ CH ₃ CHO, 3.9 μmol h ⁻¹ g ⁻¹ ; the total solar fuel production rate is 62-fold of GO	96
GO-CoPc ^g	Visible light, 20 W white cold LED flood light	CO ₂ saturated TEA ^h /H ₂ O solution	CH ₃ OH	78.8 μmol h ⁻¹ g ⁻¹ , 2-fold of GO	97
GO-phen-Ru ⁱ	Visible light, 20 W white cold LED flood light	CO ₂ saturated DMF/TEA/H ₂ O solution	CH ₃ OH	82.9 μmol h ⁻¹ g ⁻¹ , 1.8-fold of GO	98

Note: ^aMAQSP refers to multianthraquinone substituted porphyrin; ^bTEOA refers to triethanolamine; ^cIP refers to 1,1',1''-(20-(2-((7-amino-9, 10-dioxo-9, 10-dihydroanthracene-2-yl)amino)quinolin-3-yl) porphyrin-5, 10, 15-triyl) tris(quinoline-3, 2-diy))tris(indoline-2, 3-dione); ^dBODIPY refers to 1-picolylamine-2-aminophenyl-3-oxy-phenyl-4,4'-difluoro-1,3,5,7-tetramethyl-2,6-diethyl-4-bora-3a,4a-diaza-s-indacene-triazine; ^eTHPP refers to meso-tetrahydroxyphenyl porphyrin; ^fCoTHPP refers to cobalt tetrahydroxyphenyl porphyrin; ^gCoPc refers to cobalt phthalocyanine tetrasulfonamide [Co-Pc-(SO₂NH₂)₄] complex [(bpy)₂Ru(bpm)]₂RuCl₂•4PF₆; ^hTEA refers to triethylamine; ⁱRu refers to ruthenium trinuclear complex.

3.1 Graphene-semiconductor photocatalysts

Semiconductors as the most important type of photocatalysts have been intensively investigated to couple with graphene for obtaining graphene-based composites, which have been proven to display obviously improved photocatalytic performance for reduction of CO₂ than the corresponding bare semiconductors. For example, Hersam *et al.* have synthesized a series of graphene-TiO₂ P25 (solvent exfoliated graphene SEG-P25 and solvent-reduced graphene oxide SRGO-P25) composites by a vacuum filtration method for photoreduction of CO₂ to methane (CH₄).⁷⁶ As shown in **Fig. 4A**, the results show that the SEG-P25 composites with the appropriate addition of SEG exhibit a significantly higher

photoactivity that bare P25 for CO₂ reduction in the presence of H₂O vapor under both UV and visible light irradiation. The improved photoactivity of SEG-P25 is ascribed to that SEG efficiently captures and transfers the photoelectrons generated from the excitation of TiO₂, which thus inhibits the recombination of charge carriers and facilitates the reduction of CO₂ to generate CH₄. In contrast, it is notable that no improvement or limited photoactivity enhancement is observed for SRGO-P25 composites as compared with P25 under UV and visible light illumination, respectively. This is mainly because that the SRGO obtained from solvent-reduced graphene oxide possesses a high defect density and thus large sheet resistance (**Fig. 4B, C**), which is unfavorable for the photoelectrons separation and transfer. This work has

proven that (i) graphene is able to act as an efficient co-catalyst for improving the photocatalytic activity of TiO_2 for reduction of CO_2 ; (ii) the defect density and sheet resistance of graphene has significant influence on the photoactivity enhancement of the resulting graphene-semiconductor composite photocatalysts.

Additionally, Chai and co-workers have reported the synthesis of nitrogen doped- TiO_2 -001/graphene (N- TiO_2 -001/GR) composites by in situ growth of well-faceted N- TiO_2

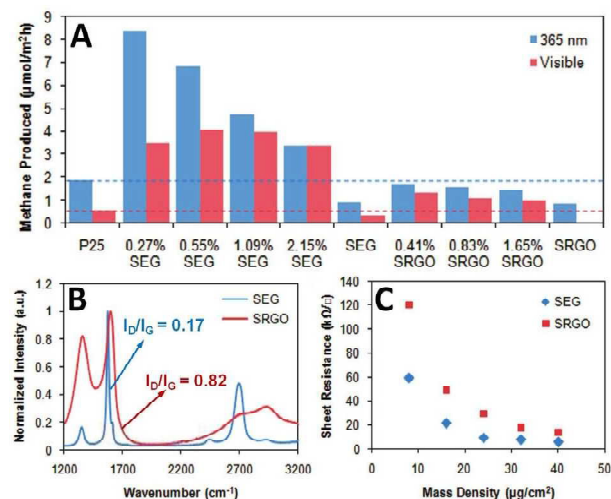


Fig. 4 Photocatalytic activity of the SEG-P25 and SRGO-P25 composites for CO_2 reduction under ultraviolet and visible illumination (A); intensity-normalized Raman spectra of SEG and SRGO films annealed at 400°C for 30 min in air (B); sheet resistances of SEG and SRGO thin films formed *via* vacuum filtration as a function of mass density (C). Reprinted with permission from ref. 76. Copyright 2011 American Chemical Society.⁷⁶

with exposed (001) facets onto GR sheets for photocatalytic reduction of CO_2 to CH_4 in the presence of H_2O vapor.⁹³ **Fig. 5A** displays the photoactivity test results over the as-synthesized samples, from which it can be seen that under visible light irradiation, the N- TiO_2 -001/GR composite exhibits the optimal CH_4 yield of $3.7\ \mu\text{mol g}_{\text{catalyst}}^{-1}$ after the reaction of 10 h, which is approximately 11-fold higher activity than that of TiO_2 -001. In addition, the photoactivity of N- TiO_2 -001/GR is also better than those of TiO_2 -001/GR, N- TiO_2 /GR, TiO_2 /GR and N- TiO_2 -001 counterparts. The high photocatalytic performance of N- TiO_2 -001/GR is primarily attributed to the effective charge transportation of graphene, large exposure of catalytic active (001) facets relative to the (101) facets and high absorption of visible light of the composite, which strongly inhibit the recombination of electron-hole pairs, and simultaneously promote the activation of CO_2 and utilization of solar energy over N- TiO_2 -001/GR,⁹³ thereby enhancing the photocatalytic reduction of CO_2 , as illustrated in **Fig. 5B**.

Apart from TiO_2 , in a subsequent work of Chai *et al.*, they have fabricated a series of sandwich-like graphene-(g- C_3N_4) (GCN) composites by one-pot impregnation-thermal reduction strategy for the conversion of CO_2 to CH_4 using H_2O vapor as a scavenger.⁷⁴ Under visible light irradiation, the

pure g- C_3N_4 without graphene displays low CH_4 production with a total yield of $2.55\ \mu\text{mol g}_{\text{catalyst}}^{-1}$ after reaction of 10 h due to rapid recombination of electron-hole pairs, as presented in **Fig. 6A, B**. By integrating g- C_3N_4 with graphene, the as-obtained GCN samples demonstrate obviously improved photoactivity for CH_4 formation. The optimal GCN-0.15 composite with the loading of 15 wt% graphene displays the maximum CH_4 production yield of $5.87\ \mu\text{mol g}_{\text{catalyst}}^{-1}$ among the GCN samples, which is 2.3-fold of the photoactivity of pure g- C_3N_4 . The enhanced photocatalytic

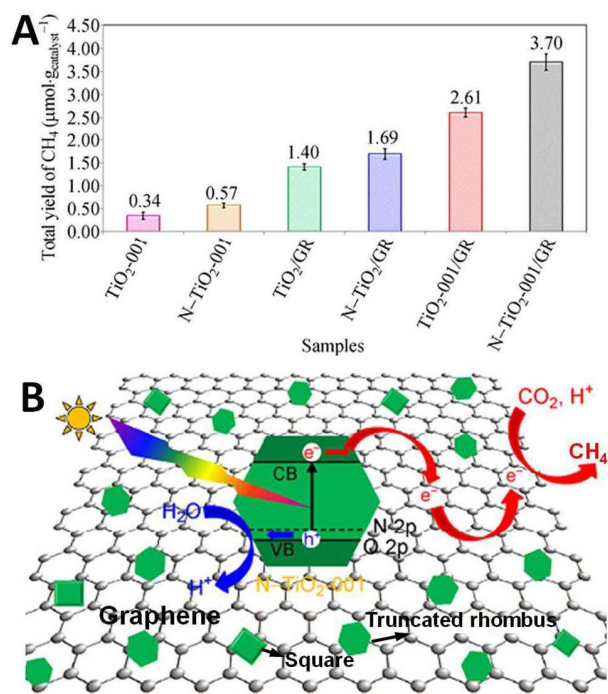


Fig. 5 Total yield of CH_4 over as-synthesized TiO_2 -001, N- TiO_2 -001 and a series of TiO_2 -based/GR nanocomposites (A); schematic illustration of the charge transfer and separation of electron-hole pairs for the reduction of CO_2 with H_2O to CH_4 using N- TiO_2 -001/GR composites under visible light irradiation (B). Reprinted with permission from ref. 93. Copyright 2014 Springer.⁹³

activity of GCN is accredited to the following concomitant factors. Firstly, the formation of C-O-C bond between graphene and g- C_3N_4 narrows the band gap of GCN and renders the GCN composites more sensitive to the visible light region, as reflected in **Fig. 6C**. Secondly, the coherent interface between graphene and g- C_3N_4 results in a more efficient electron transfer within the 2D layered composite structure (**Fig. 6D**). Finally, CO_2 molecules with delocalized π -conjugated binding π^*_s can adsorb onto the graphene surface through π - π conjugation interaction, which is beneficial for the destabilization and activation of CO_2 molecules. These factors synergistically promote the photoactivity enhancement of GNS toward visible-light-driven CO_2 reduction.⁷⁴

Additionally, CdS as another important semiconductor has also been coupled with graphene for photocatalytic reduction of CO_2 . Yu and co-workers have prepared a series of reduced

graphene oxide-CdS nanorod (RGO-CdS) composites *via* a one-step microwave-hydrothermal method in ethanolamine-water solution.⁷⁵ These composite samples have shown obviously improved visible light photocatalytic activity for reduction of CO₂ with H₂O vapor to CH₄ as compared to blank CdS. As shown in Fig. 7, the 0.5%RGO-CdS (G0.5) composite with the optimal content of RGO exhibits the highest CH₄ production rate of 2.51 μmol h⁻¹ g⁻¹, which exceeds the rate over blank CdS nanorod by more than 10 times (0.21 μmol h⁻¹ g⁻¹). Moreover, the value is also higher than that of the reference 0.5%Pt-CdS nanorod composite photocatalyst (1.52

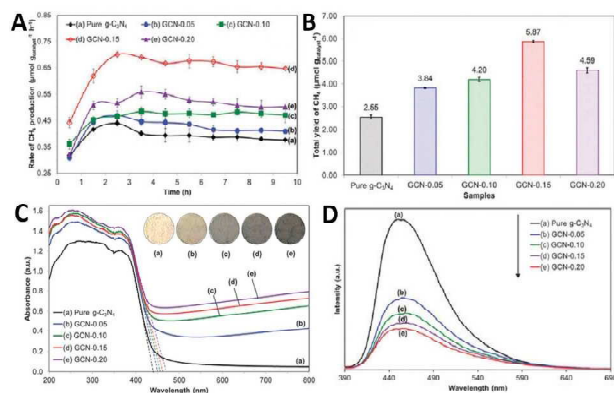


Fig. 6 Time dependence of the photocatalytic production rate of CH₄ (A) and total CH₄ yield over the as-prepared photocatalysts (B); UV-Vis DRS spectra (the inset shows the color of the photocatalysts) (C) and PL spectra (D) of pure g-C₃N₄ and GCN composites. Reprinted with permission from ref. 74. Copyright 2015 Royal Society of Chemistry.⁷⁴

μmol h⁻¹ g⁻¹) under identical reaction conditions. This high photoactivity of the RGO-CdS composites has been ascribed to the deposition of CdS nanorod onto RGO sheets, which not only promotes the separation and transfer of the

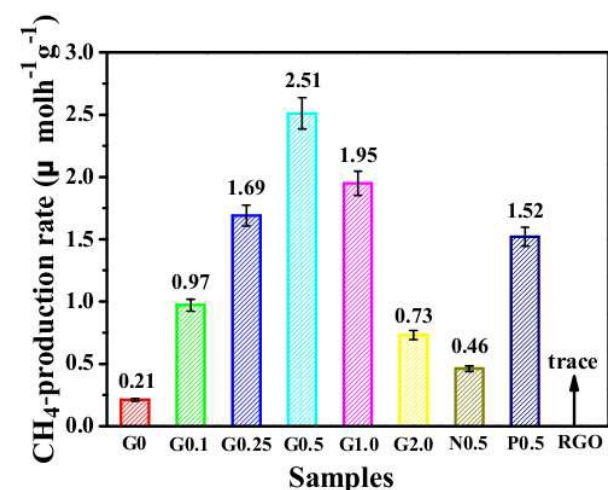


Fig. 7 Comparison of the photocatalytic CH₄ production rate of the G0, G0.1, G0.25, G0.5, G1.0, G2.0, N0.5, P0.5 and RGO samples under visible light irradiation. Reprinted with permission from ref. 75. Copyright 2015 Royal Society of Chemistry.⁷⁵

photogenerated charge carriers, but also enhances the adsorption and activation of CO₂ molecules,⁷⁵ thus resulting in the photoactivity enhancement for CO₂ reduction over the RGO-CdS composites. However, in spite of the effectiveness of RGO-CdS composites for photocatalytic reduction of CO₂ to CH₄, the photostability of the composites is still unclear. Given that the photocatalytic reduction of CO₂ over RGO-CdS composites is performed in gaseous phase without sacrificial reagent, it is natural to raise the question about the photocorrosion of semiconductor CdS in the composite, which would cause detrimental effect on the photoactivity and stability of the RGO-CdS composite photocatalysts.

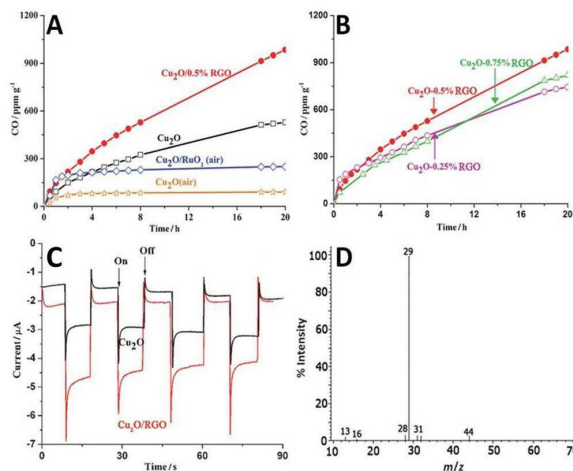


Fig. 8 Time-dependent photocatalytic conversion of CO₂ into CO over Cu₂O and Cu₂O/RGO composites (A); photocatalytic conversion of CO₂ over Cu₂O/RGO composites with different amounts of RGO (B); photocurrent response of Cu₂O and Cu₂O/RGO electrodes in 0.5 M Na₂SO₄ solution (pH = 6.8) (C); MS spectrum of the gas-phase products of ¹³CO₂ photoreduction by the Cu₂O/RGO photocatalyst (D). Reprinted with permission from ref. 80. Copyright 2014 John Wiley & Sons, Inc.⁸⁰

Moreover, Tang and co-workers have reported the photocatalytic reduction of CO₂ to CO in water over Cu₂O/reduced graphene oxide (Cu₂O/RGO) composites synthesized *via* one-step microwave-assisted hydrothermal method.⁸⁰ Before the photoactivity measurements, a thermal pretreatment of the photocatalysts in Ar or air has been performed to remove possible trace organic contaminants on the samples. Fig. 8A, B has shown the visible-light-driven catalytic reduction of CO₂ over blank Cu₂O and Cu₂O/RGO composites in the presence of sodium sulfite as hole scavenger. The result demonstrates that by coupling with RGO, the photoreduction activity of Cu₂O has been efficiently enhanced. As for the lower photoactivity of Cu₂O (Air) and Cu₂O/RuO_x (Air) than that of Cu₂O (Ar), it is attributed to the partial oxidation of Cu₂O to CuO upon heating, which causes harmful effect on the photoactivity of Cu₂O.⁸⁰ In addition, the photoactivity test also shows that the Cu₂O/0.5% RGO composite produce CO stably with an average rate of 50 ppm g⁻¹ h⁻¹ for 20 h, showing a potential for photocatalytic conversion of CO₂ over Cu₂O/RGO in a sustainable manner.

The high photocatalytic activity and stability of $\text{Cu}_2\text{O}/\text{RGO}$ composites are ascribed to the electron acceptor role of RGO, which efficiently promotes charge carriers transfer and retards the electron-hole recombination (Fig. 8C). Moreover, to further clarify the origin of the CO generated during the reaction, the photoreduction of ^{13}C -labeled CO_2 has been conducted, as shown in Fig. 8D. The dominant peak of ^{13}CO ($m/z = 29$) clearly indicates that the evolved CO originates from the photoreduction of CO_2 rather than the photodecomposition of RGO or organic contaminants that might be adsorbed on the photocatalyst surface/reactor.

Besides the reported binary graphene-semiconductor composites, some multinary (*i.e.*, ternary and quaternary) graphene-semiconductor-based photocatalysts with further improved photoactivity as compared with their binary counterparts have also been fabricated for catalytic reduction of CO_2 into solar fuels and chemicals.

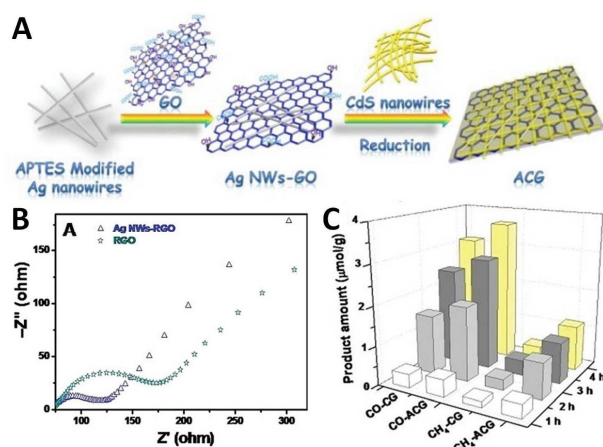


Fig. 9 Schematic illustration of the synthesis of Ag NWs-RGO-CdS NWs (ACG) hybrid structure (A); electrochemical impedance spectroscopy (EIS) Nyquist diagrams of RGO and Ag NWs-RGO (B); the amounts of CO and CH_4 formed in the photocatalytic reduction of CO_2 in the presence of H_2O vapor over the ACG and CG samples under visible light irradiation (C). Reprinted with permission from ref. 85. Copyright 2015 Royal Society of Chemistry.⁸⁵

For instance, our group has fabricated a ternary composite photocatalysts of one-dimensional (1D) silver nanowires (NWs)-doped reduced graphene oxide (RGO) integrated with CdS nanowires network *via* a simple electrostatic self-assembly method followed by a hydrothermal reduction process,⁸⁵ as illustrated in Fig. 9A. The integration of Ag NWs has significantly enhanced the electrical conductivity of RGO (Fig. 9B) by opening up new conduction channels of bridging the high resistance grain-boundaries of RGO with 1D Ag nanowires, which thus results in the more efficient separation and transfer of charge carriers of Ag NWs-RGO-CdS NWs (ACG) composite than that of RGO-CdS NWs (CG) sample.⁸⁵ As a result, the optimal ternary Ag-CdS-2%RGO exhibits much improved photoactivity for CO_2 reduction with H_2O after visible light irradiation of 4 h ($3.648 \mu\text{mol g}^{-1}$ for CO and $1.153 \mu\text{mol g}^{-1}$ for CH_4 , respectively) as compared to CdS-2%RGO ($3.115 \mu\text{mol g}^{-1}$ for CO and $0.416 \mu\text{mol g}^{-1}$ for CH_4 , respectively), as shown in Fig. 9C.

Additionally, Zou and co-workers have designed an all-solid-state Z-scheme system array consisting of $\text{Fe}_2\text{V}_4\text{O}_{13}$ nanoribbon (NR)/reduced graphene oxide (RGO)/CdS nanoparticle grown on the stainless-steel mesh (SSM) for photocatalytic conversion of CO_2 with H_2O vapor into CH_4 .⁸⁶ As shown in Fig. 10A, the SEM image shows that the as-prepared $\text{Fe}_2\text{V}_4\text{O}_{13}$ NRs with a length of 10-20 μm are perpendicularly grown on the entire SSM surface. With the GO coating and subsequent annealing treatment, the RGO-coated surface of the $\text{Fe}_2\text{V}_4\text{O}_{13}$ NR appears obvious a crumpled-layer structure (Fig. 10B). Then, after chemical vapor deposition of CdS, large numbers of the tiny CdS particles are observed on the surface of the $\text{Fe}_2\text{V}_4\text{O}_{13}/\text{RGO}$ (Fig. 10C). The SEM analysis clearly demonstrates the ordered structure and intimate interfacial contact of the three components in the resulting $\text{Fe}_2\text{V}_4\text{O}_{13}/\text{RGO}/\text{CdS}$ composite.

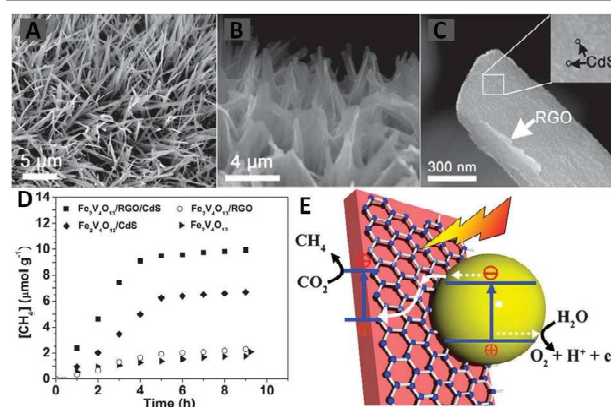


Fig. 10 SEM images of $\text{Fe}_2\text{V}_4\text{O}_{13}$ (A), $\text{Fe}_2\text{V}_4\text{O}_{13}/\text{RGO}$ (B) and $\text{Fe}_2\text{V}_4\text{O}_{13}/\text{RGO}/\text{CdS}$ (C); CH_4 evolution activities over the as-prepared sample (D); schematic illustration of photocatalytic conversion of CO_2 into CH_4 over $\text{Fe}_2\text{V}_4\text{O}_{13}/\text{RGO}/\text{CdS}$ Z-scheme system. ($\text{Fe}_2\text{V}_4\text{O}_{13}$ $E_{\text{CB}}: -0.55 \text{ eV}$, $E_{\text{VB}}: 1.28 \text{ eV}$; CdS $E_{\text{CB}}: -0.52 \text{ eV}$, $E_{\text{VB}}: 1.88 \text{ eV}$ vs. NHE). Reprinted with permission from ref. 86. Copyright 2015 Royal Society of Chemistry.⁸⁶

Fig. 10D has displayed the photocatalytic performance of bare $\text{Fe}_2\text{V}_4\text{O}_{13}$, binary $\text{Fe}_2\text{V}_4\text{O}_{13}/\text{RGO}$, $\text{Fe}_2\text{V}_4\text{O}_{13}/\text{CdS}$ and ternary $\text{Fe}_2\text{V}_4\text{O}_{13}/\text{RGO}/\text{CdS}$ toward reduction of CO_2 to CH_4 under visible light irradiation, which demonstrates that the ternary $\text{Fe}_2\text{V}_4\text{O}_{13}/\text{RGO}/\text{CdS}$ displays the highest photoactivity. The photoactivity enhancement has been ascribed to formation of efficient Z-scheme heterostructure in the ternary $\text{Fe}_2\text{V}_4\text{O}_{13}/\text{RGO}/\text{CdS}$ composite. As graphically illustrated in Fig. 10E, the photoexcited electrons from CB of CdS may transfer to RGO and release to the VB of $\text{Fe}_2\text{V}_4\text{O}_{13}$ to recombine with the existing holes of $\text{Fe}_2\text{V}_4\text{O}_{13}$. The holes stored by the CdS oxidize H_2O to O_2 , whereas the electrons stored by the $\text{Fe}_2\text{V}_4\text{O}_{13}$ reduce CO_2 to CH_4 .⁸⁶ The presence of RGO interlayer between $\text{Fe}_2\text{V}_4\text{O}_{13}$ and CdS provides a high-speed charge channel in the heterostructure due to its high electronic mobility, leading to more efficient spatial separation of the electrons and holes and subsequent promoting the high photocatalytic conversion efficiency of CO_2 .⁸⁶ Notably, in the present $\text{Fe}_2\text{V}_4\text{O}_{13}/\text{RGO}/\text{CdS}$ Z-scheme system, the holes are stored by CdS to oxidize H_2O to O_2 . However, it is well-known that the S^{2-} in CdS is easier to be

oxidized by holes than that of H₂O. Therefore, the photostability of this Z-schematic Fe₂V₄O₁₃/RGO/CdS composite photocatalysts should be concerned.

Very recently, Hou and co-workers have developed a novel quaternary three-dimensional bimetal-graphene-semiconductor (Au-Cu/graphene/Cu₂O) integrated system for solar-light-driven conversion of CO₂ into methanol,⁸⁷ in which the Cu₂O nanowire array on a Cu mesh substrate are encapsulated by ultrathin graphene layers and then

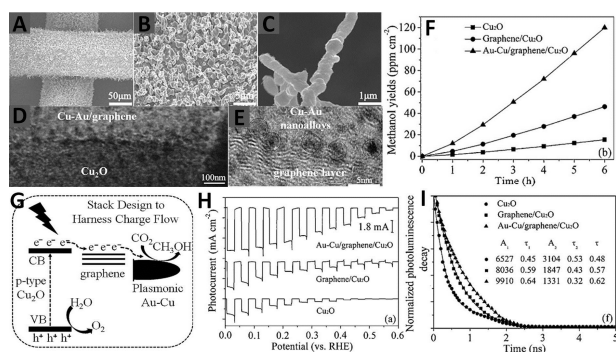


Fig. 11 SEM (A-C), TEM (D) and HRTEM (E) images of Au-Cu/graphene/Cu₂O array; photocatalytic production yield of methanol as a function of time over Cu₂O, graphene/Cu₂O, and Au-Cu/graphene/Cu₂O array photocatalysts (F); diagram of the CO₂ photoreduction mechanism for the Au-Cu/graphene/Cu₂O array (G); photoelectrochemical performance using Na₂SO₄ solution (pH = 5) with potassium phosphate (G) and time-resolved photoluminescence decay spectra (excitation λ = 420 nm) for Cu₂O, graphene/Cu₂O, and Au-Cu/graphene/Cu₂O array photocatalysts. Reprinted with permission from ref. 87. Copyright 2015 John Wiley & Sons, Inc.⁸⁷

decorated with optimized combination of Au-Cu nanoalloys, as displayed by the SEM and TEM images in **Fig. 11A-E**. The photocatalytic reduction of CO₂ over the as-synthesized composites has been performed in CO₂ saturated H₂O. As shown in **Fig. 11F**, under visible light irradiation of 6 h, the methanol yield over graphene/Cu₂O array is 46.3 ppm cm⁻² h⁻¹, which is 3-fold of the photoactivity of Cu₂O array (15.4 ppm cm⁻² h⁻¹). Especially, the Au-Cu/graphene/Cu₂O array exhibits the highest methanol yield of 120.0 ppm cm⁻² h⁻¹, which is 7.8 times higher than that of Cu₂O array. The recycle test of Au-Cu/graphene/Cu₂O shows that the yield rate of methanol from CO₂ conversion maintains 92% of its original activity after five runs, implying the high photostability of the composite. Moreover, the photoactivity of Au-Cu/graphene/Cu₂O has also been proven to be much higher than that of the graphene/Cu₂O array decorated with Au, Cu and Au + Cu prepared by step-by-step deposition of metal on the support.⁸⁷ The significantly improved photoactivity of Au-Cu/graphene/Cu₂O is attributed to that (1) the introduction of graphene as an electron conductive platform with lower energy level than the conduction band (CB) of Cu₂O leads to the photogenerated electrons migration from CB of Cu₂O to the graphene layer;⁸⁷ (2) the formation of Schottky junction in 3D Au-Cu/graphene/Cu₂O system results into the further migration of electrons from graphene to Au-Cu nanoalloys.⁸⁷ Furthermore, the electromagnetic field induced from the

surface plasmonic resonance effect of Au-Cu also promotes the migration of electrons through the harness charge flow of Cu₂O nanowire array → graphene layer → Au-Cu nanoalloys (**Fig. 11G**). Consequently, the electron-hole pairs are readily separated and the lifetime of the charge carriers is efficiently prolonged (**Fig. 11H, I**) in the quaternary 3D Au-Cu/graphene/Cu₂O composites, which become readily available to drive the multi-electron CO₂ reduction process.

3.2 Graphene-organics/biomolecule photocatalysts

Organic compounds and metal organic complexes with suitable light absorption property is another important class of promising materials that are capable of participating in photochemical charge transfer and energy transfer processes.⁹⁹⁻¹⁰² The integration of graphene with organics and metal organic complexes, such as porphyrins, phthalocyanines iron complex and ruthenium complex have also been employed to improving the efficiency for harvesting solar energy.¹⁰³⁻¹⁰⁶ Especially, some recent reports have proven that with the assistance of biological enzyme, the graphene-organics/biomolecule photocatalysts composite system are able to catalytic conversion of CO₂ to target products efficiently and selectively.⁸⁹⁻⁹¹

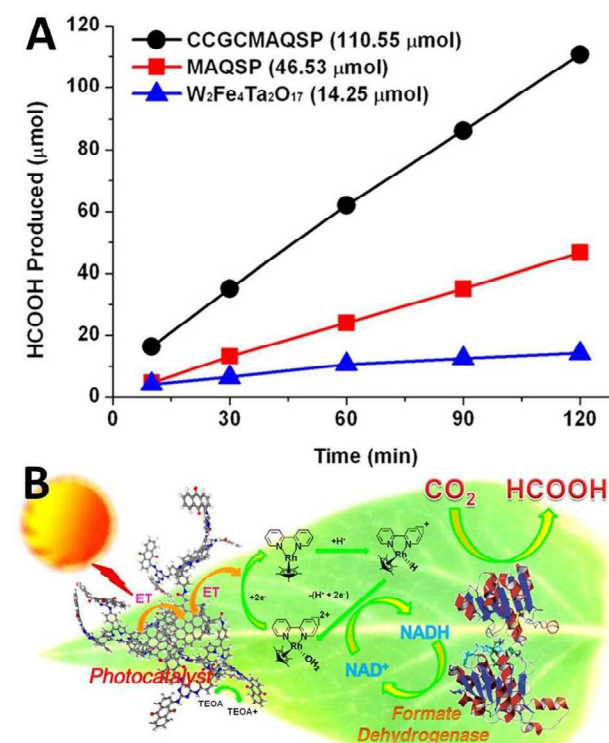


Fig. 12 Photocatalytic activities of CCGCMAQSP, MAQSP, and W₂Fe₄Ta₂O₁₇ in visible-light-driven artificial photosynthesis of formic acid from CO₂ (A); schematic illustration of artificial photosynthesis of formic acid from CO₂ over graphene-based photocatalyst catalyzed under visible light irradiation (B). Reprinted with permission from ref. 89. Copyright 2012 American Chemical Society.⁸⁹

For instance, Baeg and co-workers have designed a graphene-based photocatalyst-biocatalyst coupled system, which is consisted of chemically converted graphene coupled multianthraquinone substituted porphyrin (CCGMAQSP), organometallic rhodium complex, nicotinamide adenine dinucleotide (NADH) and formate dehydrogenase, for photocatalytic reduction of CO₂ to formic acid (HCOOH) in sodium phosphate buffer solution with triethanolamine (TEOA) as hole scavenger.⁸⁹ As shown in Fig. 12A, the HCOOH yield increases linearly with the reaction time when CCGMAQSP is used as the photocatalyst. The yield for the production of HCOOH over CCGMAQSP within 2 h is 110.55 μmol, which is much higher than the values of the reference photocatalysts of W₂Fe₄Ta₂O₁₇ (14.25 μmol) and blank MAQSP (46.53 μmol). The working mechanism of the as-prepared graphene-based photocatalyst-biocatalyst coupled system for production of formic acid from CO₂ has been schematically illustrated in Fig. 12B. Under visible light irradiation, the MAQSP firstly absorbs photons through the transition between localized orbitals around chromophore to generate electrons and transfer to the organometallic rhodium complex *via* graphene. Then, the reduced rhodium complex abstract protons from aqueous solution and further transfer electrons and hydrides to NAD⁺, which converts NAD⁺ to NADH and finishes the photocatalysis cycle. During this process, the rhodium complex shuttles as an electron mediator between CCGMAQSP photocatalyst and NAD⁺, which facilitates the regeneration of the NADH. Finally, NADH is consumed by the CO₂ substrate for its enzymatic (formate dehydrogenase) conversion to HCOOH. The NAD⁺ released from the enzyme can undergo photocatalysis cycle in the same way, leading to the photoregeneration of NADH. These two catalysis cycles thus couple integrally to work together, ultimately yielding HCOOH from CO₂.⁸⁹

In a following work of Baeg *et al.*, they have further reported the photocatalytic reduction of CO₂ to methanol over another new graphene-based photocatalyst-biocatalyst integrated system, which is derived from the covalent attachment of isatin-porphyrin (IP) chromophore onto chemically converted graphene (CCG) forming CCG-IP photocatalyst, and then coupling with enzymes.⁹⁰ The production of methanol over the as-synthesized photocatalysts has been performed in CO₂-saturated sodium phosphate buffer solution with the addition of rhodium complex, mixed enzymes (formate dehydrogenase, formaldehyde dehydrogenase and alcohol dehydrogenase) and hole scavenger of TEOA. The photoactivity test results in Fig. 13A have shown that the methanol yield of CCG-IP photocatalyst is 11.21 μM after visible light irradiation of 1 h, which is much higher than that of the reference CCGMAQSP photocatalyst (5.62 μM). In addition, the photoactivity test of the IP chromophore generates trace amount of methanol which could not be quantified, while CCG fails to produce any methanol. Fig. 13B has displayed the transient photocurrent study of IP and CCG-IP. The CCG-IP presents significantly higher photocurrent than the IP electrode. The prompt photocurrent response of CCG-IP is well accordance with its

improved photoactivity, indicating significant co-catalytic role of CCG for enhancing the electron transfer from IP to CCG upon visible light irradiation. Furthermore, the control experiments in the absence of CO₂, CCG-IP photocatalyst (but with enzymes) or visible light irradiation show that no methanol is formed in all these cases, which further confirm the photocatalytic nature of converting CO₂ to methanol over the CCG-IP composite.

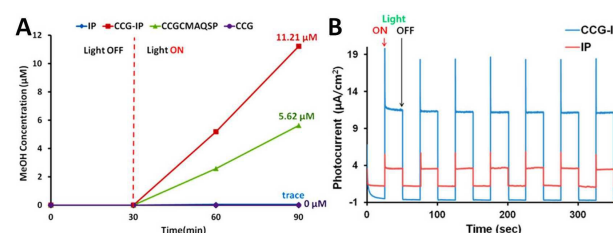


Fig. 13 Exclusive production of methanol from CO₂ under visible light by CCG-IP, CCGMAQSP, IP, and CCG upon integration with β-NAD⁺, rhodium complex, TEOA, photocatalyst, and enzymes (formate dehydrogenase, formaldehyde dehydrogenase, and alcohol dehydrogenase) in sodium phosphate buffer (A); photocurrent-time profiles of FTO/IP and FTO/CCG-IP electrodes under simulated solar light illumination (electrolyte: 0.1 M NaCl in water, bias potential: 0-0.1 V (vs Ag/AgCl)) (B). Reprinted with permission from ref. 90. Copyright 2011 American Chemical Society.⁹⁰

The above discussed works clearly demonstrate the possibility of using photoactive graphene-organics to construct photocatalyst-biocatalyst coupled system for catalytic reduction of CO₂ to value-added chemicals and fuels. More importantly, the works have shown the great potential of controlling the product with high selectivity through choosing appropriate biological enzymes. For example, in the presence of formate dehydrogenase alone, the photocatalytic conversion of CO₂ over the CCGMAQSP composite produces formic acid,⁸⁹ whereas in the case of adding mixed enzymes of formate dehydrogenase, formaldehyde dehydrogenase and alcohol dehydrogenase, methanol is detected as the exclusive products for photocatalytic conversion of CO₂ over the same CCGMAQSP photocatalyst under identical reaction condition.⁹⁰ Therefore, the design and fabrication of graphene-based photocatalysts/biomolecule composite system would be a promising strategy for selectively photocatalytic conversion of CO₂ to target products.

3.4 Graphene derivatives-based photocatalysts

In addition to the above discussed graphene-semiconductor and graphene-organics/biomolecule photocatalysts, graphene oxide (GO), the most regularly used precursor of graphene for the synthesis of graphene-based composite photocatalysts,^{29, 60} recently has also been proven to be able to perform as photocatalysts for solar energy conversion.¹⁰⁷⁻¹¹¹ In particular, the GO has demonstrated to display obvious photoactivity that comparable with traditional semiconductors such as TiO₂ for catalytic reduction of CO₂ to produce solar chemicals and fuels.

For example, Chen *et al.* have reported the photocatalytic reduction of CO₂ with H₂O vapor to CH₃OH using GO as a promising photocatalyst under simulated solar light

irradiation.⁹⁵ They have synthesized a series of GO samples under different oxidation conditions and found that the GO-3 obtained *via* the Hummers' oxidation with excess KMnO_4 and H_3PO_4 exhibits the highest photocatalytic efficiency. As shown in Fig. 14A, the photocatalytic conversion rate of CO_2 to CH_3OH on GO-3 achieves up to $0.172 \mu\text{mol g cat}^{-1} \text{h}^{-1}$, which is 6-fold higher than the pure TiO_2 P25. The isotope tracer analysis of GO with $^{13}\text{CO}_2$ demonstrates that CH_3OH is produced directly from the photocatalytic reduction of CO_2 instead of any photo-dissociation of the GO photocatalyst. Besides, the origin of the photoactivity has been described by the band structure of GO, as illustrated in Fig. 14B. In the GO photocatalyst, the oxygenated functional groups provide a 2D network of sp^2 and sp^3 bonded atoms, leading to the presence of a finite band gap depending on the isolated sp^2 domains. During the photocatalytic reduction process, the GO with surplus oxygenated components is photoexcited to generate electron-hole pairs, which then migrate to the GO surface to react with absorbed CO_2 reactants and produce CH_3OH .⁹⁵

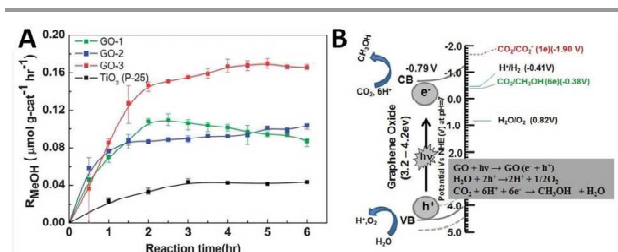


Fig. 14 Photocatalytic methanol formation (R_{MeOH}) on different GO samples (GO-1, GO-2, GO-3) and TiO_2 using a simulated solar-light source (A); schematic illustration of the photocatalytic CO_2 reduction mechanism on GO (B). Reprinted with permission from ref. 95. Copyright 2013, Royal Society of Chemistry.⁹⁵

In a subsequent work of *Chen et al.*, they have further synthesized a series of copper nanoparticles decorated GO photocatalysts with different weight ratios of Cu *via* a one-step microwave method.⁹⁶ The as-synthesized GO-Cu composites display significantly enhanced photocatalytic activity for reduction of CO_2 to methanol and acetaldehyde in the presence of H_2O vapor under visible light irradiation, as shown in Fig. 15A. The solar fuel (methanol and acetaldehyde) formation rate over the optimal Cu/GO-2 (10 % Cu) composite ($6.4 \mu\text{mol g cat}^{-1} \text{h}^{-1}$) is 60 times higher than that of pristine GO and 240 times higher than that of commercial P25 under visible light irradiation. The characterization results demonstrate that the incorporation of Cu effectively tunes the work function of GO due to the spontaneous transfer of electrons from GO to Cu nanoparticles.⁹⁶ As a result, the charge separation at the GO-Cu interface and suppression of carrier recombination is more efficient than that of GO (Fig. 15B), which thus leads to the enhanced photocatalytic CO_2 reduction activity of GO-Cu composites. In addition, the variation in the production rate of different products is suggested to be determined by the band positions

of these samples, as displayed in Fig. 15C. The plot shows that the conduction band (CB) of Cu/GO-1 (5 % Cu) and Cu/GO-2 (10 % Cu) is feasible for the multi-electron reduction of CO_2 to methanol and acetaldehyde. In contrast, the position of CB in Cu/GO-3 Cu/GO-2 (15 % Cu) is slightly lower than the $\text{CO}_2/\text{CH}_3\text{OH}$ reduction potential at around -0.35 V , which leads to the absence of methanol in the product.⁹⁶

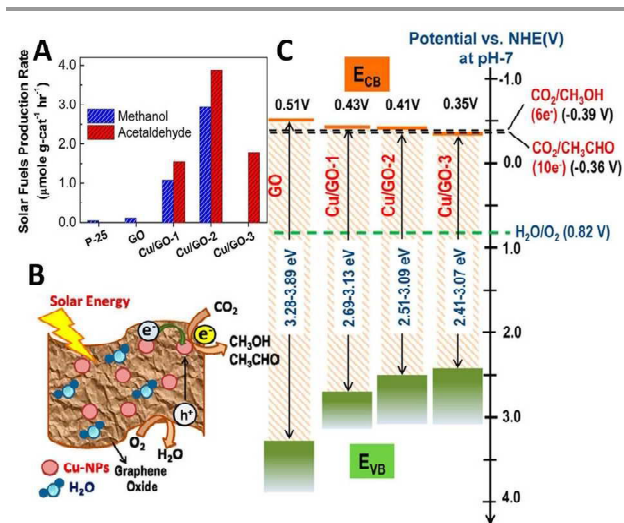


Fig. 15 Photocatalytic Solar fuel production rate for GO, and Cu/GO-1, Cu/GO-2, and Cu/GO-3 (production rate was derived following 2 h of light irradiation) (A); schematic photocatalytic reaction mechanism (B); and band-edge positions of pristine GO and Cu/GO hybrids in compared with $\text{CO}_2/\text{CH}_3\text{OH}$ and $\text{CO}_2/\text{CH}_3\text{CHO}$ formation potential (C). Reprinted with permission from ref. 96. Copyright 2014 American Chemical Society.⁹⁶

Additionally, *Jain et al.* have reported the immobilization of light responsive metal-organic complexes onto the GO support,^{97, 98, 112} which also significantly improves the photocatalytic CO_2 reduction activity of GO. For example, they have immobilized ruthenium trinuclear polyazine complexes on phenanthroline modified GO through the complex formation between them.⁹⁸ The as-synthesized Ru-(phen-GO) composite displays higher visible light photoactivity than GO for catalytic reduction of CO_2 to CH_3OH in $\text{DMF}/\text{H}_2\text{O}$ solution with the addition of triethylamine as sacrificial agent, as shown in Fig. 16A. After 48 h illumination, the CH_3OH yield of about $3978 \mu\text{mol g cat}^{-1}$ is obtained, which is much higher than the yield of CH_3OH over blank GO ($2201 \mu\text{mol g cat}^{-1}$) under identical reaction conditions. The isotopic labeling experiment performed with $^{13}\text{CO}_2$ confirms that the methanol formation through CO_2 reduction. In addition, the recycle test of continuous five runs demonstrates that the Ru-(phen-GO) composite is stable as well as efficient for the photocatalytic reduction of CO_2 under the current experimental conditions. The enhanced photocatalytic performance of Ru-(phen-GO) composites is ascribed to the significant sensitization role of the synthesized ruthenium complex. It is able to strongly absorb visible light and be excited to inject electrons into the conduction band (CB) of

GO, which subsequently reduces the adsorbed CO_2 to methanol on the surface of GO. Meanwhile, the sacrificial agent of triethylamine provides electrons to the oxidized ruthenium for the continuation of the process (Fig. 16B).⁹⁸

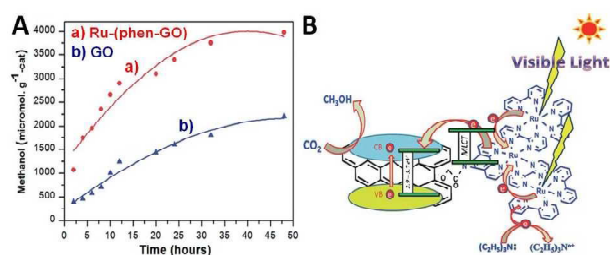


Fig. 16 Photocatalytic conversion of CO_2 to methanol over the Ru-(phen-GO) composites and GO (A); possible mechanism of photocatalytic CO_2 reduction over Ru-(phen-GO) composites (B). Reprinted with permission from ref. 98. Copyright 2014 Royal Society of Chemistry.⁹⁸

Besides the photocatalytic reduction of CO_2 over GO-based composite photocatalysts, recently, Jain *et al.* have reported that the nitrogen-doped graphene (GrN_{700}) obtained from annealing dried GO-ethylenediamine material at 700 °C under argon flow is also efficient for CO_2 reduction in DMF/ H_2O solvent.¹¹³ In particular, they have further grafted copper (II) complex $[\text{Cu}(\text{bpy})_2(\text{H}_2\text{O})_2]\text{Cl}_2 \cdot 2\text{H}_2\text{O}$ onto the nitrogen-doped graphene (GrN_{700}) structure, which efficiently improves the photocatalytic CO_2 reduction activity by a factor of 2.05. As shown in Fig. 17A, after visible light irradiation of 24 h, the methanol production over bare copper (II) complex (CuC), GO, GrN_{700} , $\text{GrN}_{700}\text{-CuC}$ and $\text{GrN}_{700}\text{:CuC}$ (physical mixture) displays a total yield of 285, 420, 780, 971 and 1600 $\mu\text{mol g}^{-1}$, respectively. The $\text{GrN}_{700}\text{-CuC}$ has shown the highest photoactivity among these samples. The blank experiment performed in N_2 atmosphere demonstrates that no obvious methanol generation has been detected, confirming that the CH_3OH is produced directly from the photocatalytic reduction of CO_2 . Moreover, the recycling experiment after five runs shows that methanol yield over $\text{GrN}_{700}\text{-CuC}$ is about 90% of its original photoactivity (Fig. 17B). These results indicate that the synthesized $\text{GrN}_{700}\text{-CuC}$ photocatalyst is quite stable and can be efficiently used for catalytic reduction of CO_2 . The possible photocatalytic mechanism over $\text{GrN}_{700}\text{-CuC}$ has been illustrated as following. In the $\text{GrN}_{700}\text{-CuC}$ composite system, the N-doped graphene performed like a semiconductor, and the copper complex with good visible light absorbance works like a photosensitizer. Under visible light irradiation, the copper bipyridine complex would photoexcited to generate electrons and then transfer the conduction band of N-doped graphene, while the holes are scavenged by the solvent.¹¹³ Due to the high electrical conductivity and large surface for the attachment of CO_2 of N-doped graphene, the electrons in the conduction band of GrN_{700} efficiently reduce the CO_2 molecules to CH_3OH .

According to the above discussed examples reported by different research groups, it is certain that the modification of graphene such as oxidation and doping would enable the

as-obtained graphene derivatives to be photocatalysts for catalytic conversion of CO_2 . However, the origin of the light driven photoactivity of the graphene oxide and nitrogen doped graphene for catalytic reduction of CO_2 is still not well understood. In addition, the photostability of the graphene derivatives-based photocatalyst, especially for the graphene oxide, is another important issue that should be carefully concerned. Because some previous works has proven that the light irradiation of GO during the photocatalytic process would result in an obvious decrease of oxygenated functional groups and thus narrows the band-gap of GO.¹¹⁴

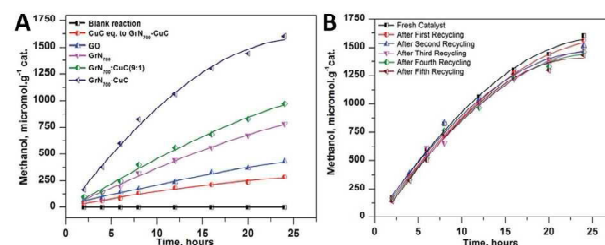


Fig. 17 Photocatalytic conversion of CO_2 into methanol using various catalytic materials under visible light irradiation (A); methanol yield from the photoreduction of CO_2 under visible irradiation using fresh and recycled $\text{GrN}_{700}\text{-CuC}$ catalyst (B). Reprinted with permission from ref. 113. Copyright 2014 Royal Society of Chemistry.¹¹³

4. Tuning the product selectivity of photocatalytic conversion of CO_2 over graphene-based photocatalysts

In addition to the photocatalytic activity, the selectivity toward target products is another important concern related to the photocatalytic conversion of CO_2 to produce solar fuels and chemicals. Recently, some reports have proven that in addition to improving the photoactivity, the integration of graphene with photoactive ingredient is also able to tune the product selectivity for photocatalytic reduction of CO_2 .

For example, Zou *et al.* have reported the fabrication of $\text{G-Ti}_{0.91}\text{O}_2$ hollow spheres consisting of molecular-scale alternating $\text{Ti}_{0.91}\text{O}_2$ nanosheets and G nanosheets for photocatalytic reduction of CO_2 .⁷⁹ As shown in Fig. 18, the total conversion of CO_2 to renewable fuels (CO and CH_4) in the presence of H_2O vapor over $\text{G-Ti}_{0.91}\text{O}_2$ hollow spheres is five-times higher than blank $\text{Ti}_{0.91}\text{O}_2$ hollow spheres and nine-times higher than commercial P25. The higher photoactivity of $\text{G-Ti}_{0.91}\text{O}_2$ hollow spheres is attributed to that: (i) the ultrathin nature of $\text{Ti}_{0.91}\text{O}_2$ nanosheets favors the rapid transportation of photoelectrons onto the surface to participate in the photoreduction; (ii) the sufficiently compact stacking of ultrathin $\text{Ti}_{0.91}\text{O}_2$ nanosheets with G nanosheets leads to the spatial separation of the charge carriers; (iii) the hollow structure allows a more efficient, permeable absorption and scattering of light. Notably, the photoactivity result has also shown that CH_4 is the major product over $\text{Ti}_{0.91}\text{O}_2$ photocatalyst, whereas CO is dominantly produced over $\text{G-Ti}_{0.91}\text{O}_2$ composites. This photoactivity difference

indicates the significant role of graphene on determining the product for photocatalytic reduction of CO₂. The possible reason has been explained as following: the formation of CO and CH₄ follows the reaction route of CO₂ → CO → C → CH₂ → CH₄ with the aid of two-electron and eight-electron transfer, respectively.⁷⁹ The transferred electrons from Ti_{0.91}O₂ to G diffuse quickly on a large area of G, benefiting from the enhanced electron mobility of G. This restrains the accumulation of the electrons and decreases local electron density, which is favorable for two-electron reaction to form CO.

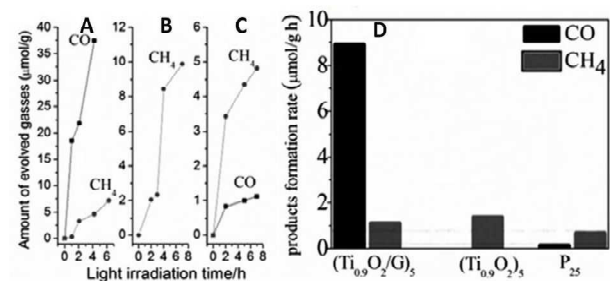


Fig. 18 Photocatalytic CH₄ (dots) and CO (squares) evolution amounts for (G-Ti_{0.91}O₂)₅ hollow spheres (A), (Ti_{0.91}O₂)₅ hollow spheres (B), and P₂₅ (C); comparison of the average product formation rates (D). Reprinted with permission from ref. 79. Copyright 2012 John Wiley & Sons, Inc.⁷⁹

In a subsequent work, Zou *et al.* have reported another graphene-TiO₂ (G-TiO₂) composites prepared by an in situ reduction-hydrolysis technique in a binary ethylenediamine (En)-H₂O solvent.⁷⁸ The reduction of GO to G by En and the formation of TiO₂ nanoparticles loaded onto G through chemical bonds (Ti-O-C bond) are achieved simultaneously.⁷⁸ In particular, owing to the reducing role of En, abundant Ti³⁺ is formed on the surface of TiO₂ in the G-TiO₂ composites. **Fig. 19A** has displayed the photocatalytic activity for reduction of CO₂ in the presence of H₂O vapor over the G-TiO₂ samples. The results show that 2%G-TiO₂ composite displays the optimal photoactivity (8 μmol g⁻¹ h⁻¹ CH₄ and 16.8 μmol g⁻¹ h⁻¹ C₂H₆), which is much better than blank TiO₂ (10.1 μmol g⁻¹ h⁻¹ CH₄ and 7.2 μmol g⁻¹ h⁻¹ C₂H₆) and commercial P₂₅ (0.69 μmol g⁻¹ h⁻¹ CH₄, and minor CO 0.16 μmol g⁻¹ h⁻¹, C₂H₆ is absent). In addition, it is notable that with the increase of weight ratio of G in the G-TiO₂ composites, the production rate of CH₄ slowly decreases while the production rate of C₂H₆ increases to some degree (**Fig. 19B, C**). This photoactivity change has been ascribed to the presence of surface-Ti³⁺ and G in the G-TiO₂ composites, which are able to couple with the •CH₃ and stabilize the •CH₃ species *via* π-conjugation between the unpaired electron of the radical and aromatic regions of the G, respectively.⁷⁸ As a result, the increasing accumulation of •CH₃ over G-TiO₂ significantly raises the opportunity of formation of C₂H₆ by the coupling of •CH₃ and restrains the combination of •CH₃ with H⁺ and e⁻ into CH₄.

Moreover, Wu *et al.* have also reported the control of photocatalytic products for reduction of CO₂ with H₂O vapor over graphene-based composites.⁹⁴ They have synthesized two types of graphene-porphyrin composite films *via* a mist spray method, for which the cobalt tetrahydroxyphenyl porphyrin (CoTHPP) and meso-tetrahydroxyphenyl porphyrin (THPP) are chosen as the light harvester due to their suitable light absorption property and high photostability. **Fig. 20A, B** displays the photoactivities of the synthesized samples, which shows that THPP/G and CoTHPP/G both present higher

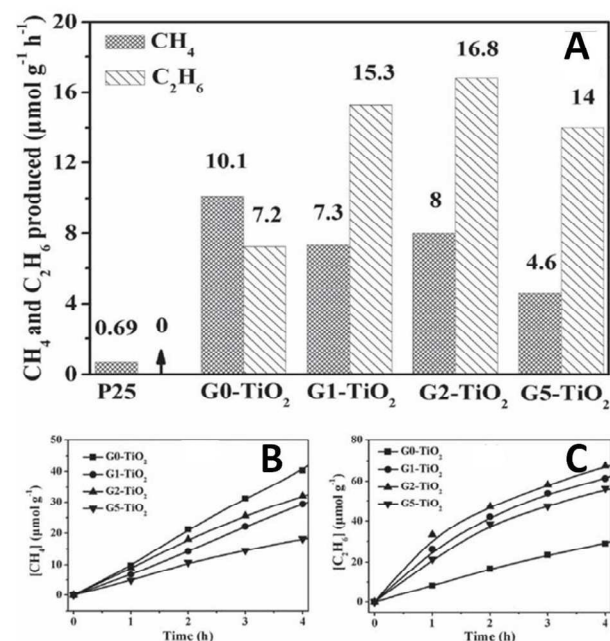


Fig. 19 Comparison of photocatalytic activity of samples G_x-TiO₂ (x = 0,1,2,5; x is the weight ratio of G in the obtained samples) and P₂₅, the molar ratio of C₂H₆ to CH₄ increases from 0.71 (for G₀-TiO₂), 2.09 (G₁-TiO₂), 2.10 (G₂-TiO₂), to 3.04 (G₅-TiO₂) (A); photocatalytic CH₄ (B) and C₂H₆ (C) evolution amounts for samples G_x-TiO₂ (x = 0, 1, 2, 5). Reprinted with permission from ref. 78. Copyright 2013 John Wiley & Sons, Inc.⁷⁸

photoactivity than their counterparts of THPP and CoTHPP in terms of the yield of hydrocarbon generation. This is mainly because that the graphene sheet with high electrical conductivity can greatly increase the lifetime of photogenerated charge carriers in the composite photocatalysts and improve the adsorption of CO₂ molecules, thereby enhancing the photoactivity of the THPP/G and CoTHPP/G composites. In addition, the control experiment of photocatalytic reduction of CO₂ over THPP and CoTHPP without graphene has shown that only very small amounts of CH₄ and trace amounts of H₂ are detected, no C₂H₂ is available. The result indicates that graphene plays a key effect on the generation of C₂H₂ in the graphene-porphyrin composite system. The possible reason has been ascribed to the outstanding ability of graphene as an excellent electron transfer mediator and adsorber for CO₂, which promotes the reduction of CO₂ on graphene. Simultaneously, H₂O is

oxidized on the porphyrin of THPP and CoTHPP, by which realizes the spatial separation of photoredox processes. Moreover, the reaction intermediates such as $\text{CO}_2^{\cdot-}$ anion radical with a delocalized electronic structure can also be attached onto graphene through π - π non-covalent bonds and receive electrons uninterrupted.⁹⁴ This would improve the stability of the reaction intermediates and enhances the coupling opportunities of them, thereby promoting the formation of C_2H_2 . As for the different photoactivity between THPP/G and CoTHPP/G, the theoretical simulation result has proposed that the structure difference in central ring of the porphyrin molecule between THPP and CoTHPP is the main reason (Fig. 20C, D). The central ring of CoTHPP molecule is not a planar structure, which breaks the large π structure and is adverse for the transfer of electrons to graphene for the reduction of CO_2 .⁹⁴ Finally, the control experiments in the presence of N_2 and heating of the catalysts at 50 °C without light have been carried out. No CH_4 and C_2H_2 can be detected in these circumstances. The result confirms that the CH_4 and C_2H_2 products are generated by the photocatalytic reduction of CO_2 over the graphene-porphyrin composites.

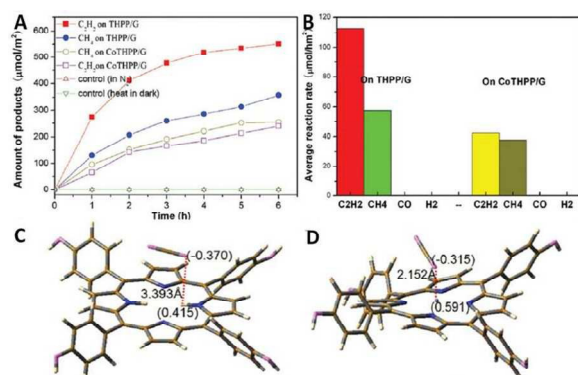


Fig. 20 Plots of hydrocarbon generation vs. time for the porphyrin-graphene catalysts obtained using the gas-solid phase reduction method (A) and corresponding hydrocarbon generation rate (B); the charge distribution and distance between the positive charges and molecules: THPP⁺ with CO_2 (C), CoTHPP⁺ with CO_2 (D). Reprinted with permission from ref. 94. Copyright 2014 Royal Society of Chemistry.⁹⁴

The above reports have obviously demonstrated the important role of graphene on tuning the product selectivity for photocatalytic reduction of CO_2 . With the incorporation of graphene, the synthesized graphene-based composite photocatalysts show great promise for converting CO_2 into more valuable high-grade multi-carbon compounds (such as C_2H_2 , C_2H_6). However, currently, there is lack of direct and detailed experimental evidences to support the proposed reaction mechanism for controlling the CO_2 reduction product by graphene. In order to deeply exploit the potential application of graphene in promoting the photocatalytic conversion of CO_2 to produce high-energy-density multi-carbon compounds, more attention and efforts should be paid to this area.

5. Summary and perspectives

In this perspective review, we have summarized the literature results on exploring efficient graphene-based photocatalysts for catalytic conversion of CO_2 into solar fuels and chemicals. The progresses achieved by different research groups in this field demonstrate that coupling graphene with photoactive materials in a suitable manner and modification of graphene itself (*e.g.*, oxidation and doping) hold great potential for improving the efficiency of photocatalytic conversion of CO_2 . However, despite the considerable developments reported in this area, there are still some fundamental and essential issues that merit more research attention.

Firstly, the photocatalytic CO_2 reduction efficiencies of most of the graphene-based composite reported to date remain unsatisfactory (the rate of product formation is measured in $\mu\text{mol g}^{-1} \text{h}^{-1}$). On-going efforts are still required to improve the overall efficiency of the CO_2 photoreduction process. In this respect, the construction of multinary graphene-based composite photocatalysts with the optimization of each component and the atomic charge carrier transfer pathway across the interface between the different components would be an effective strategy.^{29, 60} In addition, the theoretical calculations of charge carrier dynamics within the photoactive ingredients and at their interfaces with graphene are also important.

Secondly, the photostability of the graphene-based composite photocatalysts is another important problem that should be considered. During the photocatalytic reaction process, the photoelectrons will be consumed to drive CO_2 reduction half-reaction, leaving the holes in the reaction system, which would be accumulated on the surface of the photocatalysts, and then decompose the photocatalyst component. This issue would be particularly prominent when the composite photocatalysts contain metal sulfide semiconductors, graphene oxide and organics/metal organic complexes. Given this issue, the integration of high-performance water oxidation co-catalyst into the graphene-based composite photocatalysts to promote the fast consumption of photogenerated holes would be an effective way for enhancing the photoactivity and stability of the graphene-based composite photocatalysts.

Thirdly, the origin of the photocatalytic generated products of CO_2 reduction over graphene-based composites should be identified, for example, by isotopic labeling experiment with $^{13}\text{CO}_2$. This is mainly because that the organic compounds in the reaction system, such as the residues obtained from the synthesis of photoactive materials with organic precursors, can be the origin of the observed products or at least can contribute in a certain percentage to the products. Moreover, considering the peculiar nature of the graphene-based composite photocatalysts with the carbon source of graphene, it is especially significant and necessary to confirm the origin of the products. However, a lot of the studies commented in this review have neglected this confirmation.

Finally, the underlying photocatalytic mechanism for reduction of CO_2 over graphene-based photocatalysts, and in particular, the reaction mechanism of graphene on tuning the

product selectivity of photocatalytic conversion of CO₂ should be clarified in detail. In this regard, the experimental and computational methods, such as in situ time-resolved spectroscopy (time-resolved fluorescence spectroscopy and femtosecond transient absorption spectroscopy), electron paramagnetic resonance spectroscopy and density functional theory calculations²⁰ should be integratively employed. The rational understanding of the mechanism would in turn offers guided information to design more efficient and highly selective graphene-based composites to promote the conversion of CO₂ with sunlight.

Acknowledgements

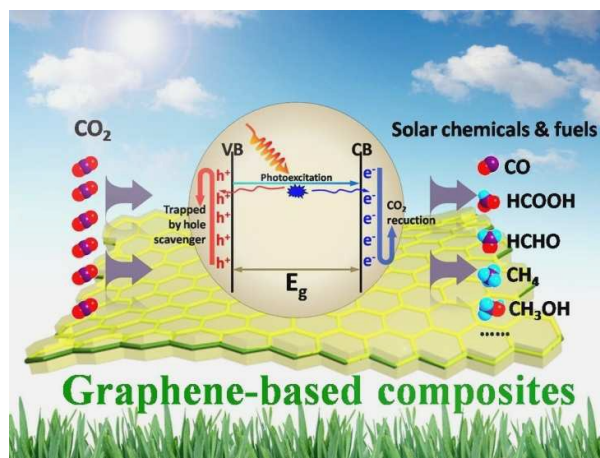
The support from the Key Project of National Natural Science Foundation of China (U1463204), the National Natural Science Foundation of China (20903023 and 21173045), the Award Program for Minjiang Scholar Professorship, the Natural Science Foundation of Fujian Province for Distinguished Young Investigator Grant (2012J06003), the Independent Research Project of State Key Laboratory of Photocatalysis on Energy and Environment (No. 2014A05), the first Program of Fujian Province for Top Creative Young Talents, and the Program for Returned High-Level Overseas Chinese Scholars of Fujian province is kindly acknowledged.

Notes and references

- S. N. Habisreutinger, L. Schmidt-Mende and J. K. Stolarczyk, *Angew. Chem. Int. Ed.*, 2013, **52**, 7372-7408.
- P. D. Tran, L. H. Wong, J. Barber and J. S. C. Loo, *Energy Environ. Sci.*, 2012, **5**, 5902-5918.
- N. S. Lewis and D. G. Nocera, *Proc. Natl. Acad. Sci. U. S. A.*, 2006, **103**, 15729-15735.
- D. C. Grills and E. Fujita, *J. Phys. Chem. Lett.*, 2010, **1**, 2709-2718.
- J. J. Concepcion, R. L. House, J. M. Papanikolas and T. J. Meyer, *Proc. Natl. Acad. Sci. U. S. A.*, 2012, **109**, 15560-15564.
- S. C. Roy, O. K. Varghese, M. Paulose and C. A. Grimes, *ACS Nano*, 2010, **4**, 1259-1278.
- H. Tong, S. Ouyang, Y. Bi, N. Umezawa, M. Oshikiri and J. Ye, *Adv. Mater.*, 2012, **24**, 229-251.
- T. Inoue, A. Fujishima, S. Konishi and K. Honda, *Nature*, 1979, **277**, 637-638.
- X. Chen, C. Li, M. Gratzel, R. Kostecki and S. S. Mao, *Chem. Soc. Rev.*, 2012, **41**, 7909-7937.
- N. Zhang, R. Ciriminna, M. Pagliaro and Y.-J. Xu, *Chem. Soc. Rev.*, 2014, **43**, 5276-5287.
- C. Chen, W. Ma and J. Zhao, *Chem. Soc. Rev.*, 2010, **39**, 4206-4219.
- J. C. Colmenares and R. Luque, *Chem. Soc. Rev.*, 2014, **43**, 765-778.
- M. R. Hoffmann, S. T. Martin, W. Choi and D. W. Bahnemann, *Chem. Rev.*, 1995, **95**, 69-96.
- X. Lang, X. Chen and J. Zhao, *Chem. Soc. Rev.*, 2014, **43**, 473-486.
- S. Navalón, A. Dhakshinamoorthy, M. Álvaro and H. Garcia, *ChemSusChem*, 2013, **6**, 562-577.
- A. Corma and H. Garcia, *J. Catal.*, 2013, **308**, 168-175.
- W. Fan, Q. Zhang and Y. Wang, *Phys. Chem. Chem. Phys.*, 2013, **15**, 2632-2649.
- K. Mori, H. Yamashita and M. Anpo, *RSC Adv.*, 2012, **2**, 3165-3172.
- M. Anpo, *J. CO₂ Util.*, 2013, **1**, 8-17.
- L. Yuan and Y.-J. Xu, *Appl. Surf. Sci.*, 2015, **342**, 154-167.
- L. Jing, W. Zhou, G. Tian and H. Fu, *Chem. Soc. Rev.*, 2013, **42**, 9509-9549.
- C. Han, M.-Q. Yang, B. Weng and Y.-J. Xu, *Phys. Chem. Chem. Phys.*, 2014, **16**, 16891-16903.
- R. Asahi, T. Morikawa, H. Irie and T. Ohwaki, *Chem. Rev.*, 2014, **114**, 9824-9852.
- N. Zhang, S. Liu and Y.-J. Xu, *Nanoscale*, 2012, **4**, 2227-2238.
- G. Liu, H. G. Yang, J. Pan, Y. Q. Yang, G. Q. Lu and H.-M. Cheng, *Chem. Rev.*, 2014, **114**, 9559-9612.
- R. Leary and A. Westwood, *Carbon*, 2011, **49**, 741-772.
- Y. H. Ng, S. Ikeda, M. Matsumura and R. Amal, *Energy Environ. Sci.*, 2012, **5**, 9307-9318.
- K. S. Novoselov, A. K. Geim, S. V. Morozov, D. Jiang, Y. Zhang, S. V. Dubonos, I. V. Grigorieva and A. A. Firsov, *Science*, 2004, **306**, 666-669.
- N. Zhang, M.-Q. Yang, S. Liu, Y. Sun and Y.-J. Xu, *Chem. Rev.*, 2015, **115**, 10307-10377.
- M. J. Allen, V. C. Tung and R. B. Kaner, *Chem. Rev.*, 2010, **110**, 132-145.
- S. Stankovich, D. A. Dikin, G. H. B. Dommett, K. M. Kohlhaas, E. J. Zimney, E. A. Stach, R. D. Piner, S. T. Nguyen and R. S. Ruoff, *Nature*, 2006, **442**, 282-286.
- K. S. Novoselov, V. I. Falko, L. Colombo, P. R. Gellert, M. G. Schwab and K. Kim, *Nature*, 2012, **490**, 192-200.
- A. K. Geim, *Science*, 2009, **324**, 1530-1534.
- A. K. Geim and K. S. Novoselov, *Nat Mater*, 2007, **6**, 183-191.
- Y. Zhang, Z.-R. Tang, X. Fu and Y.-J. Xu, *ACS Nano*, 2010, **4**, 7303-7314.
- M.-Q. Yang, X. Pan, N. Zhang and Y.-J. Xu, *CrystEngComm*, 2013, **15**, 6819-6828.
- X. Xie, K. Kretschmer and G. Wang, *Nanoscale*, 2015, **7**, 13278-13292.
- Y. Zhang, Z.-R. Tang, X. Fu and Y.-J. Xu, *ACS Nano*, 2011, **5**, 7426-7435.
- N. Zhang, Y. Zhang, X. Pan, M.-Q. Yang and Y.-J. Xu, *J. Phys. Chem. C*, 2012, **116**, 18023-18031.
- J. Zhang, F.-X. Xiao, G. Xiao and B. Liu, *Nanoscale*, 2014, **6**, 11293-11302.
- A. Ye, W. Fan, Q. Zhang, W. Deng and Y. Wang, *Catal. Sci. Technol.*, 2012, **2**, 969-978.
- M.-Q. Yang, B. Weng and Y.-J. Xu, *Langmuir*, 2013, **29**, 10549-10558.
- B. Liu, L. Tian and Y. Wang, *ACS Appl. Mater. Interfaces*, 2013, **5**, 8414-8422.
- H. Zhang, X. Lv, Y. Li, Y. Wang and J. Li, *ACS Nano*, 2010, **4**, 380-386.
- W. Fan, Q. Lai, Q. Zhang and Y. Wang, *J. Phys. Chem. C*, 2011, **115**, 10694-10701.
- L. Yuan, M.-Q. Yang and Y.-J. Xu, *Nanoscale*, 2014, **6**, 6335-6345.
- M.-Q. Yang, Y. Zhang, N. Zhang, Z.-R. Tang and Y.-J. Xu, *Sci. Rep.*, 2013, **3**, 3314.
- M.-Q. Yang and Y.-J. Xu, *J. Phys. Chem. C*, 2013, **117**, 21724-21734.
- N. Zhang, M.-Q. Yang, Z.-R. Tang and Y.-J. Xu, *ACS Nano*, 2014, **8**, 623-633.
- C. Han, Z. Chen, N. Zhang, J. C. Colmenares and Y.-J. Xu, *Adv. Funct. Mater.*, 2015, **25**, 221-229.

- 51 M. Gao, C. K. N. Peh, W. L. Ong and G. W. Ho, *RSC Adv.*, 2013, **3**, 13169-13177.
- 52 X. Cao, G. Tian, Y. Chen, J. Zhou, W. Zhou, C. Tian and H. Fu, *J. Mater. Chem. A*, 2014, **2**, 4366-4374.
- 53 B. Qiu, M. Xing and J. Zhang, *J. Am. Chem. Soc.*, 2014, **136**, 5852-5855.
- 54 A. Iwase, Y. H. Ng, Y. Ishiguro, A. Kudo and R. Amal, *J. Am. Chem. Soc.*, 2011, **133**, 11054-11057.
- 55 X. Pan, M.-Q. Yang, Z.-R. Tang and Y.-J. Xu, *J. Phys. Chem. C*, 2014, **118**, 27325-27335.
- 56 Y. Zhang, N. Zhang, Z.-R. Tang and Y.-J. Xu, *ACS Nano*, 2012, **6**, 9777-9789.
- 57 N. Zhang, Y. Zhang, M.-Q. Yang, Z.-R. Tang and Y.-J. Xu, *J. Catal.*, 2013, **299**, 210-221.
- 58 F.-X. Xiao, J. Miao and B. Liu, *J. Am. Chem. Soc.*, 2014, **136**, 1559-1569.
- 59 M.-Q. Yang and Y.-J. Xu, *Phys. Chem. Chem. Phys.*, 2013, **15**, 19102-19118.
- 60 M.-Q. Yang, N. Zhang, M. Pagliaro and Y.-J. Xu, *Chem. Soc. Rev.*, 2014, **43**, 8240-8254.
- 61 N. Zhang and Y.-J. Xu, *CrystEngComm*, 2016, **18**, 24-37.
- 62 G. Xie, K. Zhang, B. Guo, Q. Liu, L. Fang and J. R. Gong, *Adv. Mater.*, 2013, **25**, 3820-3839.
- 63 X. An and J. C. Yu, *RSC Adv.*, 2011, **1**, 1426-1434.
- 64 P. V. Kamat, *J. Phys. Chem. Lett.*, 2011, **2**, 242-251.
- 65 N. Zhang, Y. Zhang and Y.-J. Xu, *Nanoscale*, 2012, **4**, 5792-5813.
- 66 Q. Xiang, B. Cheng and J. Yu, *Angew. Chem. Int. Ed.*, 2015, **54**, 11350-11366.
- 67 J. Low, J. Yu and W. Ho, *J. Phys. Chem. Lett.*, 2015, **6**, 4244-4251.
- 68 J. R. Bolton, *Science*, 1978, **202**, 705-711.
- 69 F.-X. Xiao, J. Miao, H. B. Tao, S.-F. Hung, H.-Y. Wang, H. B. Yang, J. Chen, R. Chen and B. Liu, *Small*, 2015, **11**, 2115-2131.
- 70 S. Liu, Z.-R. Tang, Y. Sun, J. C. Colmenares and Y.-J. Xu, *Chem. Soc. Rev.*, 2015, **44**, 5053-5075.
- 71 L. Yuan, M.-Q. Yang and Y.-J. Xu, *J. Mater. Chem. A*, 2014, **2**, 14401-14412.
- 72 L.-L. Tan, S.-P. Chai and A. R. Mohamed, *ChemSusChem*, 2012, **5**, 1868-1882.
- 73 B. Weng, M.-Q. Yang, N. Zhang and Y.-J. Xu, *J. Mater. Chem. A*, 2014, **2**, 9380-9389.
- 74 W.-J. Ong, L.-L. Tan, S.-P. Chai and S.-T. Yong, *Chem. Commun.*, 2015, **51**, 858-861.
- 75 J. Yu, J. Jin, B. Cheng and M. Jaroniec, *J. Mater. Chem. A*, 2014, **2**, 3407-3416.
- 76 Y. T. Liang, B. K. Vijayan, K. A. Gray and M. C. Hersam, *Nano Lett.*, 2011, **11**, 2865-2870.
- 77 Y. T. Liang, B. K. Vijayan, O. Lyandres, K. A. Gray and M. C. Hersam, *J. Phys. Chem. Lett.*, 2012, **3**, 1760-1765.
- 78 W. Tu, Y. Zhou, Q. Liu, S. Yan, S. Bao, X. Wang, M. Xiao and Z. Zou, *Adv. Funct. Mater.*, 2013, **23**, 1743-1749.
- 79 W. Tu, Y. Zhou, Q. Liu, Z. Tian, J. Gao, X. Chen, H. Zhang, J. Liu and Z. Zou, *Adv. Funct. Mater.*, 2012, **22**, 1215-1221.
- 80 X. An, K. Li and J. Tang, *ChemSusChem*, 2014, **7**, 1086-1093.
- 81 A. Wang, X. Li, Y. Zhao, W. Wu, J. Chen and H. Meng, *Powder Technol.*, 2014, **261**, 42-48.
- 82 P.-Q. Wang, Y. Bai, P.-Y. Luo and J.-Y. Liu, *Catal. Commun.*, 2013, **38**, 82-85.
- 83 X. Li, Q. Wang, Y. Zhao, W. Wu, J. Chen and H. Meng, *J. Colloid Interface Sci.*, 2013, **411**, 69-75.
- 84 L.-L. Tan, W.-J. Ong, S.-P. Chai and A. R. Mohamed, *Appl. Catal., B*, 2015, **166-167**, 251-259.
- 85 S. Liu, B. Weng, Z.-R. Tang and Y.-J. Xu, *Nanoscale*, 2015, **7**, 861-866.
- 86 P. Li, Y. Zhou, H. Li, Q. Xu, X. Meng, X. Wang, M. Xiao and Z. Zou, *Chem. Commun.*, 2015, **51**, 800-803.
- 87 J. Hou, H. Cheng, O. Takeda and H. Zhu, *Angew. Chem.*, 2015, **127**, 8600-8604.
- 88 X.-J. Lv, W.-F. Fu, C.-Y. Hu, Y. Chen and W.-B. Zhou, *RSC Adv.*, 2013, **3**, 1753-1757.
- 89 R. K. Yadav, J.-O. Baeg, G. H. Oh, N.-J. Park, K.-j. Kong, J. Kim, D. W. Hwang and S. K. Biswas, *J. Am. Chem. Soc.*, 2012, **134**, 11455-11461.
- 90 R. K. Yadav, G. H. Oh, N.-J. Park, A. Kumar, K.-j. Kong and J.-O. Baeg, *J. Am. Chem. Soc.*, 2014, **136**, 16728-16731.
- 91 R. K. Yadav, J.-O. Baeg, A. Kumar, K.-j. Kong, G. H. Oh and N.-J. Park, *J. Mater. Chem. A*, 2014, **2**, 5068-5076.
- 92 M. Xing, F. Shen, B. Qiu and J. Zhang, *Sci. Rep.*, 2014, **4**, 6341.
- 93 W.-J. Ong, L.-L. Tan, S.-P. Chai, S.-T. Yong and A. Mohamed, *Nano Res.*, 2014, **7**, 1528-1547.
- 94 T. Wu, L. Zou, D. Han, F. Li, Q. Zhang and L. Niu, *Green Chem.*, 2014, **16**, 2142-2146.
- 95 H.-C. Hsu, I. Shown, H.-Y. Wei, Y.-C. Chang, H.-Y. Du, Y.-G. Lin, C.-A. Tseng, C.-H. Wang, L.-C. Chen, Y.-C. Lin and K.-H. Chen, *Nanoscale*, 2013, **5**, 262-268.
- 96 I. Shown, H.-C. Hsu, Y.-C. Chang, C.-H. Lin, P. K. Roy, A. Ganguly, C.-H. Wang, J.-K. Chang, C.-I. Wu, L.-C. Chen and K.-H. Chen, *Nano Lett.*, 2014, **14**, 6097-6103.
- 97 P. Kumar, A. Kumar, B. Sreedhar, B. Sain, S. S. Ray and S. L. Jain, *Chem.—Eur. J.*, 2014, **20**, 6154-6161.
- 98 P. Kumar, B. Sain and S. L. Jain, *J. Mater. Chem. A*, 2014, **2**, 11246-11253.
- 99 M. L. Marin, L. Santos-Juanes, A. Arques, A. M. Amat and M. A. Miranda, *Chem. Rev.*, 2012, **112**, 1710-1750.
- 100 C. G. Silva, A. Corma and H. Garcia, *J. Mater. Chem.*, 2010, **20**, 3141-3156.
- 101 M. Alvaro, E. Carbonell, B. Ferrer, F. X. Llabrés i Xamena and H. Garcia, *Chem.—Eur. J.*, 2007, **13**, 5106-5112.
- 102 M. A. Nasalevich, M. van der Veen, F. Kapteijn and J. Gascon, *CrystEngComm*, 2014, **16**, 4919-4926.
- 103 P. Wang, N. M. Dimitrijevic, A. Y. Chang, R. D. Schaller, Y. Liu, T. Rajh and E. A. Rozhkova, *ACS Nano*, 2014, **8**, 7995-8002.
- 104 M. Zhu, Z. Li, B. Xiao, Y. Lu, Y. Du, P. Yang and X. Wang, *ACS Appl. Mater. Interfaces*, 2013, **5**, 1732-1740.
- 105 M. Zhu, Y. Dong, B. Xiao, Y. Du, P. Yang and X. Wang, *J. Mater. Chem.*, 2012, **22**, 23773-23779.
- 106 L. Shen, L. Huang, S. Liang, R. Liang, N. Qin and L. Wu, *RSC Adv.*, 2014, **4**, 2546-2549.
- 107 T.-F. Yeh, F.-F. Chan, C.-T. Hsieh and H. Teng, *J. Phys. Chem. C*, 2011, **115**, 22587-22597.
- 108 K. Krishnamoorthy, R. Mohan and S.-J. Kim, *Appl. Phys. Lett.*, 2011, **98**, 244101.
- 109 T.-F. Yeh, J.-M. Syu, C. Cheng, T.-H. Chang and H. Teng, *Adv. Funct. Mater.*, 2010, **20**, 2255-2262.
- 110 T.-F. Yeh, C.-Y. Teng, S.-J. Chen and H. Teng, *Adv. Mater.*, 2014, **26**, 3297-3303.
- 111 T.-F. Yeh, J. Cihlář, C.-Y. Chang, C. Cheng and H. Teng, *Mater. Today*, 2013, **16**, 78-84.
- 112 P. Kumar, A. Bansiwal, N. Labhsetwar and S. L. Jain, *Green Chem.*, 2015, **17**, 1605-1609.
- 113 P. Kumar, H. P. Mungse, O. P. Khatri and S. L. Jain, *RSC Adv.*, 2015, **5**, 54929-54935.
- 114 Y. Matsumoto, M. Koinuma, S. Ida, S. Hayami, T. Taniguchi, K. Hatakeyama, H. Tateishi, Y. Watanabe and S. Amano, *J. Phys. Chem. C*, 2011, **115**, 19280-19286.

TOC graphic

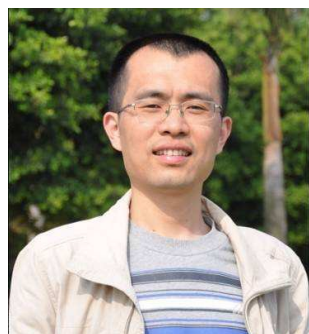


A critical summary and insight of recent advances for photocatalytic reduction of CO₂ to produce solar fuels and chemicals over graphene-based photocatalysts has been presented, with the purpose of describing the current status and promoting further development in this area.

Biographies



Min-Quan Yang is a Ph.D. student of Prof. Yi-Jun Xu at State Key Laboratory of Photocatalysis on Energy and Environment, College of Chemistry, Fuzhou University, P. R. China. His main research interests focus on the synthesis of carbon-based materials, especially graphene-based composites for applications in heterogeneous photocatalysis.



Yi-Jun Xu is a full professor now working at State Key Laboratory of Photocatalysis on Energy and Environment, College of Chemistry, Fuzhou University, P. R. China. His current research interests primarily focus on the assembly and applications of semiconductor-based nanostructured materials, such as graphene-based, one dimension-based, and core-shell-based composite photocatalysts, in heterogeneous photocatalysis.